Optimizing Trabectedin Therapy for the Treatment of Ewing Sarcoma

By

Matthew Harlow

Dissertation

Submitted to the Faculty of the

Graduate School of Vanderbilt University

in partial fulfillment of the requirements

for the degree of

DOCTOR OF PHILOSOPHY

In

Cancer Biology

August 31, 2017

Nashville, Tennessee

Approved:
Wael El-Rifai M.D., Ph.D (committee chair)
Stephen Brandt, M.D.
Michael Freeman, Ph.D.
William Tansey, Ph.D.
Patrick Grohar, M.D., Ph.D. (advisor)

ACKNOWLDEGEMENTS

First and foremost, I have to thank the people that have supported throughout my scientific career. My girlfriend, Bridget, for the love, support, and patience over the last 5 years. Without her forcing me to take time off and go on trips, I may have lost sight of the things that are important to me outside of lab, including her. My parents, Sid and Joanne, have always supported me, and I will always be indebted to them. They refused to let me become complacent as I was growing up and I believe it has inspired me down this career path. My brother, Tyler, taught me to have thick skin, which is necessary in a profession, like science, that has such a high attrition rate.

The studies detailed here have my name on the title page, but would have been completely impossible without the help of many other people. I have to thank my mentor, Dr. Grohar, for providing not only the resources, but the guidance and pathologic optimism that I needed during my tenure in the lab. Dr. Grohar taught me more than any graduate school course could (and generally in much fewer words). His ability to frame the clinical problem, and use laboratory tools to solve said problem will last with me as long as I am involved in research. I would not have been as successful if I had joined any other lab.

In addition to Dr. Grohar's guidance, he was also keenlyy aware that a good lab environment is necessary for productivity. With that in mind, I have to thank the numerous members of the Grohar lab (current and former) for their help along the way. These members include: Nichole Maloney, Christy Osgood, Joel Everett, Susan Goosen, Elissa Boguslawski, Matthew Easton, Penny Berger, Guillermo Flores, Maggie

Chasse, Jennifer Jess, and Katie Sorensen. This group of people assembled by Dr. Grohar made me want to be in lab all day, every day.

TABLE OF CONTENTS

Page

LIST OF FIGURES

Page

LIST OF ABBREVIATIONS

(In order of appearance)

IHC - immunohistochemistry

MSC - mesenchymal stem cell

EWSR1 - Ewing sarcoma breakpoint region 1

ETS - E26 transformation specific

FLI1 - friend leukemia virus integration site 1

FISH - fluorescence in-situ hybridization

qRT-PCR - quantitative real-time polymerase chain reaction

MEFs - mouse embryonic fibroblasts

Ara-C - Cytosine arabinoside

NER - nucleotide excision repair

HR - homologous recombination

MLS - myxoid liposarcoma

C_{max} - maximum concentration of drug in serum

PTM - post-translational modification

IP - immunoprecipitation

HEK - human embryonic kidney cells

UV - ultraviolet light

γH2AX - phosphorylated histone variant H2A.X

AUC - area under the curve

Chapter 1

Introduction

Ewing sarcoma

Incidence, pathology, and treatment

Ewing sarcoma is the second most common (~250 cases per year) malignant bone tumor of childhood (1). Ewing sarcoma has a peak incidence in the second decade of life, and is rarely diagnosed in patients over 30 years of age. While there has been 1 documented case of siblings with Ewing sarcoma, there is currently no published evidence to suggest that Ewing sarcoma is a heritable condition (2).

Ewing sarcoma was initially characterized as “diffuse endothelioma of the bone” by Dr. James Ewing in 1921 based on astute clinical observations (3). Dr. Ewing noted that a subset of patients diagnosed with osteosarcoma responded particularly well to radiation therapy, even though osteosarcoma was known to be resistant to this treatment strategy. He also made important observations pertaining to the site of tumor formation and the histology of the tumor cells, which aided in the differential diagnosis of what eventually became known as Ewing sarcoma (3). Dr. Ewing noted common sites for tumor involvement are in the shaft of the long bones, but rarely the ends of the bone. In addition, he wrote that patients commonly present in the clinic because of persistent, intractable bone pain that is a consequence of the osteolytic nature of the lesions (4, 5).

Under the microscope, Ewing sarcoma cells appear as sheets of small round cells with a high nuclear to cytoplasmic ratio. The cytoplasm commonly contains glycogen and the nuclei are rounded with multiple nucleoli per nucleus. Unlike other small round

cell tumors, Ewing sarcoma tumors do not produce a desmoplastic or collagenous stroma (6, 7).

Due to the large number of tumor types that are described as small, round, blue cell tumors, immunohistochemical (IHC) staining is often employed to aid in diagnosis. While the exact cell of origin in Ewing sarcoma is currently unknown, the absence of definitive differentiation markers and the fact that tumors are often found in developing bone suggests Ewing sarcoma tumors arise from a poorly differentiated stem or progenitor cell. The current hypothesis is Ewing sarcoma tumors form from early neuroectodermal or mesenchymal stem cell (MSC) lineage (6). *In silico* and *in vitro* experiments have demonstrated that the genetic profile of Ewing sarcoma cells clusters with MSCs and provides an explanation for the observed adipogenic and osteogenic differentiation phenotypes seen in cell culture (8).

CD99 is the most common IHC marker used in Ewing sarcoma and indicates a neuroectodermal origin; however, depending on the degree of differentiation, a panel of markers for a variety of lineages can be utilized (9). Aside form CD99 expression, Ewing sarcoma cells display additional features of cells originating from the neuroectodermal lineage including expression of key neurodevelopmental genes and a proclivity to migrate and invade numerous other tissues (10, 11).

Despite the classification of Ewing sarcoma as a unique disease entity and the advances in clinical diagnostics, survival rates before the introduction of chemotherapy remained low (approximately 10%) (12). Modern therapeutic regimens that include surgery, high-dose radiation therapy, and chemotherapy have achieved cure rates that approach 50% (13). However, the cure rate is dramatically affected by the presence of

unfavorable prognostic factors. The most unfavorable prognostic factor is the presence of metastatic disease at diagnosis, which affects 25% of patients (12). While lymph node and central nervous system metastases are very rare, patients who have pulmonary metastases, have a slightly more positive prognosis than patients with bone marrow metastases (12). In addition, younger patients tend to have a better prognosis than older patients (12).

Patients with Ewing sarcoma are treated with a multidrug chemotherapy regimen that consists of alternating cycles of vincristine, doxorubicin, cyclophosphamide, and ifosfamide and etoposide (14). This regimen, when administered on a compressed schedule has dramatically improved survival for patients with small primary tumors to almost 80% (5 or 10 year overall survival) (15). However, there has been no improvement in survival for patients with metastatic disease. In addition, this therapeutic strategy is accompanied by local and systemic side effects including fatigue, hair loss, nausea, vomiting, myelosuppression, cardiotoxicity, nephrotoxicity, and difficult-to-treat second malignancies (16-18). Considering the side effects of the current standard of care and the lack of improved survival for patients with metastatic disease, there is an obvious need for more effective and less toxic therapies for Ewing sarcoma patients.

The Ewing sarcoma genome

In order to develop better therapies for Ewing sarcoma patients, it is critical to understand the underlying cause and pathogenesis of the disease. Many groups have recently performed whole genome or transcriptome sequencing experiments (19-21). These studies examined Ewing sarcoma patient tumor samples paired with normal tissue as a control along with numerous Ewing sarcoma cell lines. Overall, the results of

these experiments revealed a very stable genome. Similar to many other pediatric malignancies, the somatic mutation frequency in Ewing sarcoma (0.15-0.65 mutations per Mb) is very low (22). Chromosomal gains and losses were identified in a number of patients, including gains of chr8, chr12, and the long arm of chr1 and loss of the long arms of chr9 and chr16. The chromosomal losses were less frequently identified than the chromosomal gains, and the chromosomal gains were associated with a much poorer prognosis (21). In particular, Ewing sarcoma tumors that gain the long arm of chromosome 1 over-express the DTL protein leading to defects in cell cycle regulation (23).

From these same sequencing studies, two genes were found to be recurrently mutated, TP53 and STAG2. TP53 loss of function has been identified as a common feature in the majority of human malignancies, and leads to increased genomic instability and metastatic potential (24). The spectrum of missense and frame-shift mutations identified in the TP53 gene in Ewing sarcoma patients cluster in the DNA-binding domain and lead to decreased protein expression (19, 20).

STAG2 was also identified as a recurrently mutated gene in Ewing sarcoma, but much less is known about the function of STAG2 as compared to TP53. STAG2 protein is an integral component of the cohesin complex and its inactivation by truncating mutations has been associated with aneuploidy in cancer (25). All identified STAG2 variants identified in Ewing sarcoma tumors correlated with loss of protein expression or function (19, 20). In one study, STAG2 mutations were also correlated with a higher number of chromosome structural variants (21). Interestingly, both TP53 and STAG2 genes displayed a higher mutation frequency after treatment. This implies that the

current standard of care, which includes a panel of generally cytotoxic chemotherapies and no targeted therapies, can increase the mutational burden of Ewing sarcoma patients (19).

The only genomic alteration identified in 100% of Ewing sarcoma patients is a balanced chromosomal translocation that fuses the N-terminal transactivation domain of the Ewing Sarcoma Breakpoint Region 1 (EWSR1) gene upstream of the C-terminal DNA-binding domain of an ETS (E26 transformation specific) transcription factor family member (26). The most common translocation is t(11;22)(q24;q12) which involves the 5' portion of the EWSR1 gene and the 3' portion of the friend leukemia virus integration site 1 (FLI1) gene (Figure 1) (26).

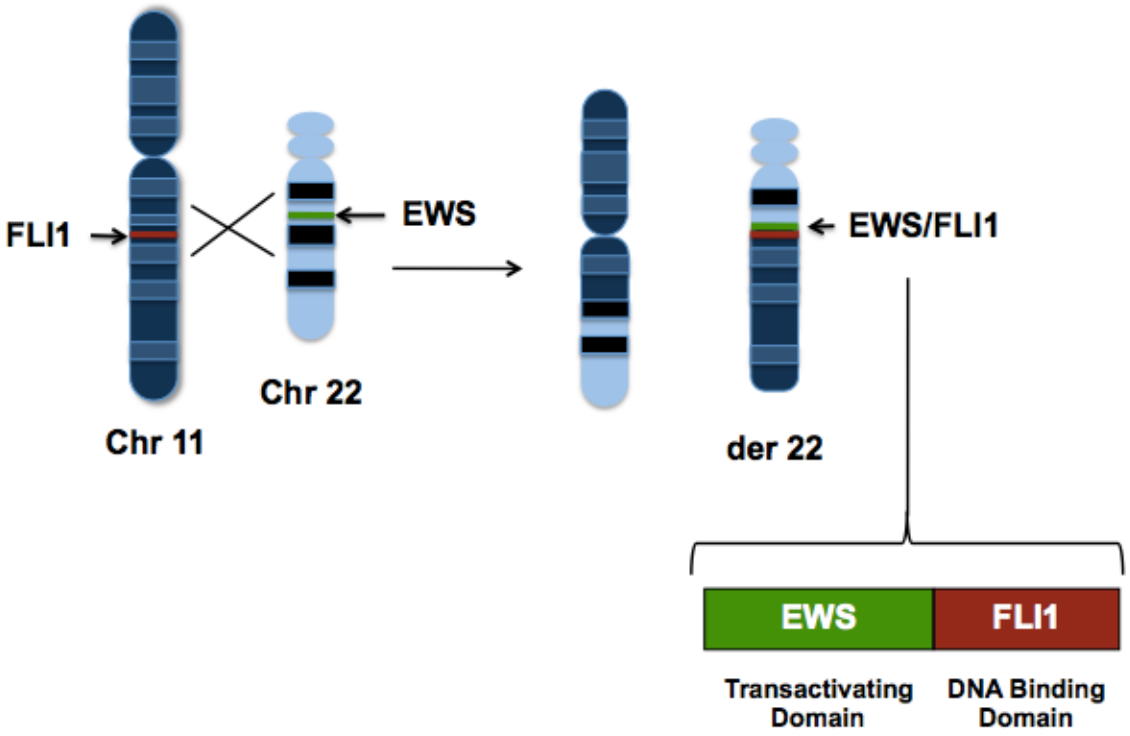

Figure 1: EWS/FLI1 translocation and protein product. The t(11;22)(q24;q12) chromosomal translocation leads to the generation of an oncogenic transcription factor, EWS/FLI1 containing the N-terminal transactivation domain of EWSR1 and the DNA-binding domain of FLI1.

The function of FLI1 has been extensively researched as a member of the ETS family of transcription factors. FLI1 protein is considered to function as a classic transcription factor that regulates the expression of critical target genes for the proper development of blood vessels and platelets (27, 28). Much less is known about the function of EWSR1 protein. Wild-type EWSR1 is thought to function at the level of transcription and RNA processing as a consequence of its DNA-binding zinc finger domain and dual RNA-binding domains (29). The N-terminus of EWSR1 contains a very potent transcriptional activation domain that is highly unstructured and predicted to mediate important protein-protein interactions (30, 31). The fusion of these two genes by chromosomal translocation leads to the generation of an oncogenic transcription factor (26).

While EWS/FLI1 is found in 85% of Ewing sarcoma tumors, 15% of Ewing sarcoma tumors are defined by fusion of EWSR1 to ETS family members that closely resemble FLI1, including ERG (10% of tumors), ETV4, ETV1, or FEV1 (32). Importantly, the discovery of EWS/ETS translocations has allowed for the definitive diagnosis of Ewing sarcoma by either fluorescence in-situ hybridization (FISH) or reverse transcriptase quantitative polymerase chain reaction (qRT-PCR).

EWS/FLI1 function and activity

EWS/FLI1 is the major oncogenic driver of disease in Ewing sarcoma (33). Similar to other driver oncogenes, EWS/FLI1 protein expression is only tolerated in a context specific manner (34). When EWS/FLI1 expression is enforced in non-transformed primary cells or mouse embryonic fibroblasts (MEFs), cells undergo apoptosis as detected by the presence of cleaved caspase 3 (35). However, when expressed in the

correct context EWS/FLI1 is oncogenic. Specifically, EWS/FLI1 can transform a variety of mesenchymal cell lines of both human and mouse origin thereby confirming its oncogenic potential (33, 34, 36-39). Oncogenesis induced by EWS/FLI1 has also been observed in a number of *in vivo* models. Upon the induction of EWS/FLI1 expression in mice under control of the Mxl-Cre promoter, 100% of mice developed leukemia, but not Ewing sarcoma (40). Additionally, mosaic expression of EWS/FLI1 in zebrafish resulted in the appearance of tumors that histologically resembled Ewing sarcoma (41).

EWS/FLI1 enforces a transcriptional program that promotes proliferation and suppresses differentiation (42-44). The transcriptional activity of EWS/FLI1 is dependent upon the capacity of the fusion protein to bind DNA at GGAA repeat sequences called micro-satellites (45). Because GGAA sequences repeat 15-40 times, multiple EWS/FLI1 proteins can bind DNA to form oligomers, create more accessible chromatin, and recruit transcriptional co-activators, such as p300 (46). As a consequence of this pioneering activity, EWS/FLI1 establishes novel enhancers that up-regulate a unique gene expression profile. As opposed to binding at GGAA microsatellites, EWS/FLI1 can also bind to DNA at single GGAA sequences (46). Upon EWS/FLI1 binding to single GGAA-sequences, wild-type ETS transcription factors are competitively displaced and transcription at these sites is repressed (45, 47, 48). In addition, the EWS/FLI1 protein is considered to be constitutively activated due to the elimination of all known negative regulatory domains identified to date in wild type EWSR1 and FLI1 proteins (49, 50).

In total, EWS/FLI1 dysregulates over 500 genes that carry out cellular processes integral to tumor initiation and disease progression (46, 51). The genes repressed by EWS/FLI1 binding are thought to be important for the differentiation potential of Ewing

sarcoma cells, cell cycle arrest, and apoptosis induction, such as TGFB2, IGFBP3, CDKN1A, and LOX (44, 52-54). EWS/FLI1-induced genes include genes that drive cellular proliferation, cell cycle progression, and maintain a de-differentiated state, such as IGF1, CCND1, EZH2, and SOX9 (55-58). Overall, the ability of EWS/FLI1 to suppress mesenchymal differentiation and promote cellular proliferation is critical in the pathogenesis of Ewing sarcoma.

Importantly, Ewing sarcoma cells depend on the continued activity of EWS/FLI1 to remain viable. Multiple independent laboratories have shown, *in vitro* and *in vivo,* that knockdown of EWS/FLI1 expression is not compatible with cellular proliferation and leads to a more stem-like phenotype (8, 52, 59, 60). In addition, upon knockdown of EWS/FLI1 expression Ewing sarcoma cells can be manipulated to differentiate into numerous mesenchymal lineages including bone, cartilage, and adipose (8, 61). These data unambiguously define EWS/FLI1 as the dominant oncogene that molecularly defines and drives progression of Ewing sarcoma. Notably, expression of EWS/FLI1 protein is an exclusive property of Ewing sarcoma cells, which provides a unique therapeutic target.

Approaches to the therapeutic targeting of Ewing sarcoma

Because of the specific expression of EWS/FLI1 in Ewing sarcoma cells and the known dependency of Ewing sarcoma cells on continued EWS/FLI1 activity, many groups have tried to target the fusion protein using a wide variety of approaches. In theory, this treatment strategy would be less toxic than the current standard of care that does not specifically target EWS/FLI1 expression or activity (14). Unfortunately,

EWS/FLI1 is a transcription factor that poses a number of problems when attempting to develop a small molecule inhibitor.

As previously mentioned, EWS/FLI1 is an aberrant transcription factor that is composed of a highly disordered N-terminal transactivation domain and a DNA-binding domain that is conserved among the 28 ETS transcription factor family members (62). The highly disordered nature of the N-terminal portion of EWS/FLI1 is proposed to mediate numerous protein-protein interactions, but has hampered the ability to obtain high-resolution crystal structures of the protein. Without a crystal structure, the development of compounds that could potentially bind to and interfere with the function of EWS/FLI1 has been unsuccessful (63-65). Compounds that interact with the C-terminal ETS DNA-binding domain have been identified, but due to the conserved nature of this region with 27 other proteins that are expressed in every tissue, they are likely to cause significant off-target effects (66, 67). For these reasons, there are currently no small molecule compounds that directly bind to and block EWS/FLI1 activity.

Another treatment option that has been pursued for Ewing sarcoma is the development of compounds that suppress the expression of EWS/FLI1. It is well known that with the loss of EWS/FLI1 protein expression, by siRNA, shRNA, or antisense oligonucleotides, Ewing sarcoma cells cannot proliferate (8, 52, 59, 60). Elimination of EWS/FLI1 protein using these methods is very effective *in vitro*; however, efficacy of siRNA therapy *in vivo* has been unsuccessful thus far due to problems associated with siRNA stability and delivery (68). While most laboratories have abandoned efforts to

target EWS/FLI1 expression by siRNA, many groups continue to search for small molecule compounds that lead to decreased EWS/FLI1 expression (69, 70).

Stegmaier et al. performed an EWS/FLI1 gene signature based screen of over 1,000 small molecules to identify compounds that reversed the genetic signature of EWS/FLI1 (71). Cytosine arabinoside (Ara-C) was identified as the top hit and was subsequently shown to function as an inhibitor of EWS/FLI1 protein expression. The decrease in EWS/FLI1 expression led to decreased Ewing sarcoma cell growth *in vitro* and *in vivo* (71). Unfortunately, Ara-C demonstrated minimal clinical benefit in patients in the Phase II setting due to off-target hematologic toxicities (13). In order to avoid the off-target toxicities associated with Ara-C administration, other groups have given the drug at lower concentrations for longer durations (72). Regrettably, this schedule of administration resulted in disease progression after less than 3 cycles of therapy.

Another therapeutic avenue that has been explored in Ewing sarcoma is to target the downstream effectors induced by EWS/FLI1 activity rather than targeting the transcription factor specifically (73). Numerous genes whose expression are both driven by EWS/FLI1 and important for the pathogenesis of Ewing sarcoma have been identified including IGF1R, PRKCB1, ID2, and BCL11B (74-77). Additionally, many of the critical EWS/FLI1 target genes identified have inhibitors that are currently in clinical development for other indications. Unfortunately, these inhibitors and this therapeutic strategy have not translated into positive clinical outcomes in Ewing sarcoma.

Because EWS/FLI1 has no known enzymatic function, it must directly interact and work in concert with many other proteins to elicit its oncogenic phenotype. EWS/FLI1 has been shown to directly bind to proteins that are essential for all aspects of

transcription including chromatin remodeling complexes, the RNA Polymerase II complex, transcriptional elongation machinery, and the spliceosome (78). Disruption of EWS/FLI1 with its interacting partner proteins by small molecule therapy has been shown to decrease Ewing sarcoma cell viability, decrease invasive potential, and slow xenograft growth in mice (65, 79, 80). To date, these compounds have failed as single therapies or have been unable to achieve the therapeutic suppression of EWS/FLI1 in early clinical trials (81, 82).

As opposed to the previously described approaches that assume EWS/FLI1 is an "undruggable" target, direct inhibition of EWS/FLI1 activity is a promising alternative to improve patient survival (83). To this end, our laboratory has taken on the challenge of identifying small molecule inhibitors of EWS/FLI1 activity. We have identified two lead compounds and second-generation analogs of mithramycin and trabectedin that are effective at reversing the gene signature of EWS/FLI1 at clinically relevant concentrations (84, 85).

The first EWS/FLI1 inhibitor that we identified was mithramycin. Mithramycin was identified by a high-throughput screen that directly assayed EWS/FLI1 activity measured by a cell-based luciferase reporter linked to the well-characterized EWS/FLI1 target gene promoter, NR0B1 (85). In order to rank the positive hits from the primary screen, a gene signature secondary screen was performed which measured the effect of drug treatment on multiple EWS/FLI1 target genes. Both the primary and secondary screens contained controls to ensure that general transcription was not affected by drug treatment. Mithramycin was the lead compound identified and treatment of Ewing sarcoma cells with mithramycin led to the reversal of EWS/FLI1 activity *in vitro* and *in*

vivo. This suppression translated into the suppression of tumor growth in two xenograft models of Ewing sarcoma.

Unfortunately, mithramycin suffers from a narrow therapeutic window in patients (Grohar et al *in press*). Therefore, our laboratory has identified structural analogs that can be administered at higher concentrations without toxicity or can achieve the same inhibitory effect on EWS/FLI1 at lower concentrations (86).

Trabectedin

Trabectedin Activity and Structure

Trabectedin is a marine natural product whose antitumor activity was first observed in the late 1960s when crude extracts from *Ecteinascidia turbinate* were found to have anti-proliferative properties (87). However, due to the low concentration (<0.002% wet weight) in turbinate extracts and the poor sensitivity of NMR protocols, isolation and structural characterization of trabectedin was not successfully performed until 1990 (88). Initial attempts to commercialize the compound were focused on aquaculture methodologies instead of synthetic processes because of the complex structure of trabectedin. As a consequence of environmental concerns, development of a protocol to synthetically produce trabectedin was pursued. These efforts resulted in the first total synthesis of trabectedin in 1996 (89).

The three-ring (Rings A-C) structure of trabectedin is unique to ecteinascidins; however, structural similarities are shared with microbial saframycins (90). The A and B rings are composed of two fused tetrahydroisoquinoline rings, which are optimal for binding to the minor groove of DNA at GC-rich sequences. The C ring of trabectedin is

another tetrahydroisoquinoline ring structure that is uniquely positioned to extend away from the DNA (Figure 2).

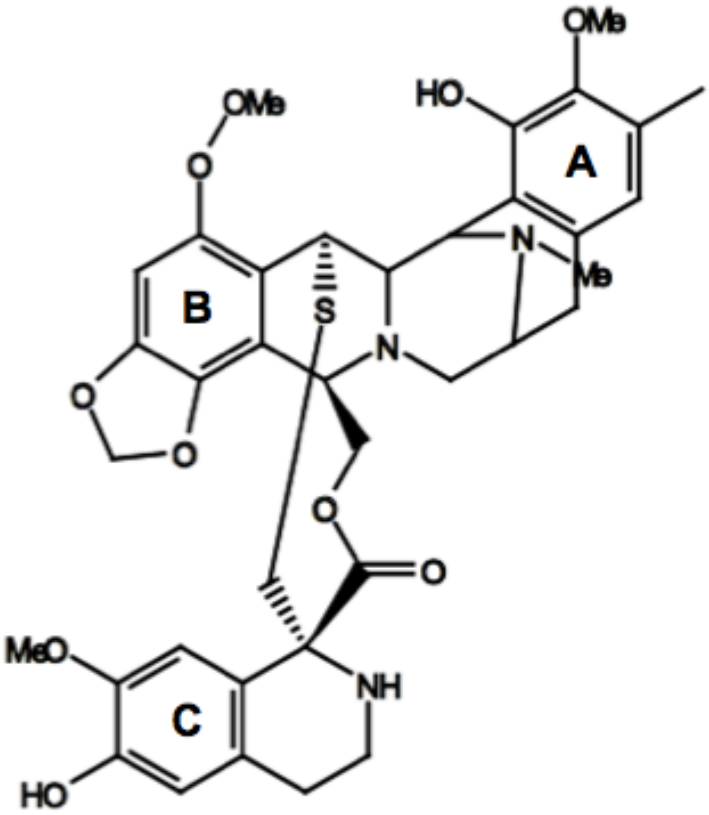

Figure 2: Structure of Trabectedin. Trabectedin is displayed here with the A, B, and C rings labeled.

The ability of trabectedin to bind and alkylate DNA leads to the formation of stable DNA adducts, which are inefficiently repaired and generate DNA damage (91). Traditionally, alkylating agents bind DNA at guanine residues in the major groove at the N7 or O6 position. Unlike traditional alkylating agents, trabectedin reversibly binds the N2 position of guanines in the minor groove (92). The binding of trabectedin to DNA has been shown to cover 3-5 bases and is strongest when the central guanine residue is flanked on the 3' side by another guanine. In addition, trabectedin bound to DNA

creates a unique bend towards the major groove that has not been identified for any other compound (93).

After the mechanism of DNA sequence specific binding was elucidated, David-Cordonnier et al. identified the specific hydroxyl group that dictates trabectedin binding to DNA (94). ET-745, a structural analog of trabectedin that is missing the critical A-ring C21 hydroxyl group, was used to demonstrate a complete loss of binding. In addition, they identified that DNA binding is necessary but not sufficient for peak anti-tumor activity of these compounds (94). The results of these studies demonstrate that the optimal activity of trabectedin, as defined by cytotoxicity, requires a ternary complex consisting of DNA, trabectedin, and an additional non-DNA target.

While the A and B rings of trabectedin have been well studied with respect to the mechanism of DNA binding, the function of the C-ring is more complex and not completely understood (95). Surprisingly, structural analogs of trabectedin lacking the C-ring still have the potential to bind DNA leading to cell death (94). In fact, C-ring deficient analogs have been shown to be more potent *in vitro* suggesting that the C-ring functions to partially mitigate the cytotoxic effects of the A and B rings (96).

Because the C-ring protrudes away from the DNA, it has been proposed to affect the function of DNA binding factors important for transcription or DNA damage repair. The most well characterized example of this phenomenon involves the ERCC5 (also known as XPG) protein, which is involved in the nucleotide excision repair (NER) pathway (97-101). ERCC5 is an endonuclease that plays a structural and catalytic role in the repair of DNA damage. ERCC5 forms a complex with the proteins XPA and RPA that stabilize the activated NER complex. This complex subsequently cleaves and

removes damaged DNA that is replaced by the DNA replication machinery (102). It has been hypothesized that the effect of trabectedin on the NER pathway is due to a trapping mechanism that creates a ternary complex involving trabectedin-DNA-NER protein, which cannot be efficiently repaired and leads to cell death (97). This mechanism requires an intact NER pathway and is unique to trabectedin treatment, as other DNA alkylating agents are hypersensitive to NER dysfunction. In agreement with this mechanism, NER-deficient cell lines are more than two-fold resistant to trabectedin treatment (97, 103).

More recently, it has been demonstrated that the DNA lesions created by trabectedin are repaired through the homologous recombination (HR) pathway (91, 104). These data demonstrate that the mechanism of cytotoxicity induced by trabectedin is dependent on proper recruitment of NER proteins, leading to NER poisoning and the creation of DNA single-strand breaks. Upon replication of DNA, single-strand breaks are converted into double stranded breaks that are more efficiently repaired by the HR machinery. This mechanism also explains why cells that are deficient in any aspect of HR are hypersensitive to trabectedin treatment (104).

Trabectedin and Transcriptional Regulation

In addition to DNA repair, transcription factor activity is affected by the C-ring of trabectedin. Activity of transcription factors, such as the E2F family, can be inhibited by trabectedin treatment (105). Additionally, many of the tumor types that routinely respond to trabectedin therapy depend on the activity of oncogenic transcription factors for survival (106-109). In support of a direct effect of trabectedin treatment on the activity of oncogenic transcription factors, Forni et al. demonstrated the loss of binding of the

FUS/CHOP transcription factor in myxoid liposarcoma (MLS) cells following trabectedin treatment (110). In agreement with this data and overwhelming *in vitro*, *in vivo*, and clinical trial data, trabectedin was approved as a second-line therapy for patients with myxoid liposarcoma in 2016 (111).

Trabectedin has also demonstrated activity in other translocation-positive soft tissue sarcomas, including synovial sarcoma and Ewing sarcoma (107, 109, 112). Our laboratory has been particularly interested in the clinical activity of trabectedin in Ewing sarcoma because of the complete response of a patient with widely metastatic disease during Phase I testing (112). While the efficacy of trabectedin was not the primary endpoint of this clinical trial, it is noteworthy that two Ewing sarcoma patients responded to single agent therapy after failing the conventional chemotherapeutic regimen. In order to explain the extreme response, our laboratory initially demonstrated that trabectedin selectively blocks the function of EWS/FLI1 (84). The inhibition of EWS/FLI1 activity was evident at the promoter level and by gene set enrichment analysis. Unfortunately, a negative Phase II trial of trabectedin in Ewing sarcoma patients was reported shortly thereafter, which stalled further clinical development (113). In light of the positive Phase I trial and the negative Phase II trial, the goal of my research has been to provide an explanation of the disparate outcomes.

Optimizing the Activity of Trabectedin in Ewing Sarcoma

The goal of this research is to optimize the on-target (EWS/FLI1 inhibitory) activity of trabectedin treatment. We believe that this can be achieved by numerous approaches including determining the specific mechanism of action of trabectedin on EWS/FLI1, establishing the optimal scheduling of trabectedin, and by discovering novel structural analogs of trabectedin that maintain on-target activity with less off-target toxicity. An

additional method to optimize the effect of trabectedin is to define novel combination therapies to specifically target Ewing sarcoma cells. Our lab has subsequently identified a synergistic combination therapy with trabectedin and irinotecan that achieves prolonged EWS/FLI1 activity suppression (114). The synergy observed with this combination is focused around the ability of trabectedin to suppress EWS/FLI1 activity, which causes a specific gene expression change that sensitizes Ewing sarcoma cells to irinotecan treatment.

This thesis will directly address our efforts to identify the specific mechanism of trabectedin-mediated EWS/FLI1 inhibition that we believe involves transient re-localization of EWS/FLI1 to the nucleolus. In addition, we believe that contrasting clinical trial results can be explained by differences in the schedule of administration between Phase I and II clinical trials. We will show that the adjusted Phase II schedule led to serum concentrations (C_{max}) of trabectedin that do not induce EWS/FLI1 re-localization. Finally, we will establish a second-generation EWS/FLI1 inhibitor, lurbinectedin, which maintains suppression of EWS/FLI1 activity at similar concentrations to trabectedin *in vitro*. However, we believe that lurbinectedin is significantly less toxic *in vivo* based on the C_{max} that can be achieved in patients before producing off-target toxicities.

Chapter 2

Identifying the Trabectedin-mediated Mechanism of EWS/FLI1 Inhibition

Introduction

Trabectedin belongs to tetrahydroisoquinoline family of small molecules that display a wide range of biological activities, including antitumor and antimicrobial effects (115). The specific activity of each molecule is thought to be a result of the structural variations that are found in each sub-family classification. Trabectedin is a member of the Ecteinascidins sub-family and displays the most potent antitumor activity of any tetrahydroisoquinoline discovered to date (115).

The first biological activity of trabectedin was reported in 1970. In these initial experiments, extracts from the Caribbean tunicate, *Ecteinascidin turbinata*, were used to treat mouse leukemia cells (87). Other groups confirmed the activity of these extracts in a large number of cancer types with limited mechanistic insights.

The first hypothesis regarding the mechanism of action was not reported until the structure of trabectedin was characterized in 1990 (116). These studies demonstrated that trabectedin's A-ring is strikingly similar to another tetrahydroisoquinoline, saframycin A. Saframycin A is a natural product that was first isolated from *Streptomyces lavendulae* in the late 1970s and studied due to its antimicrobial properties (117). Subsequently, saframycin A was shown to possess antitumor activity mediated by the ability to bind DNA in the minor groove (118). Because the purification of trabectedin was laborious and the final yield per extract was low (<0.002%), the

mechanistic studies of trabectedin were hampered until the total synthesis was published in 1996 (89).

Soon after the published synthesis, the A and B rings of trabectedin were shown to alkylate DNA in the minor groove in a manner similar to saframycin A (92). The alkylation of DNA by trabectedin bends the minor groove towards the major groove, which is unique compared to other DNA alkylating agents. Trabectedin has also been shown to poison topoisomerase I, disassemble microtubule structures, and degrade RNA polymerase II leading to transcriptional and cell cycle perturbations (119-123). These mechanisms are assumed to be off-target effects of trabectedin treatment because the concentration of trabectedin necessary to elicit these phenotypes (1-5 micromolar) *in vitro* is far beyond concentrations that are attainable in animal models or patients (10-20 nanomolar).

In addition to the presumed off-target effects of trabectedin treatment referenced above, trabectedin has demonstrated striking activity at clinically relevant concentrations in select tumor types (111). The mechanism of action at these concentrations is likely due to more specific, targeted effects of trabectedin therapy on specific oncogenic driver mutations (124). Because saframycin A and trabectedin have nearly identical binding properties and saframycin A has not demonstrated activity in the clinic, the presence of the C-ring in trabectedin is probably responsible for the increase in activity. Interestingly, many of the tumor types that are responsive to trabectedin therapy are characterized by a chromosomal translocation that generates an oncogenic transcription factor including MLS and Ewing sarcoma. The implication from these

observations is that the C-ring of trabectedin is important for modulating the activity of select transcription factors such as FUS/CHOP in MLS or EWS/FLI1 in Ewing sarcoma.

The oncogenic fusion protein in MLS, FUS/CHOP, functions analogously to EWS/FLI1 in Ewing sarcoma. FUS/CHOP regulates a unique transcriptional profile that drives proliferation and specifically blocks mesenchymal progenitor cells from progressing along the adipogenic pathway (125). When MLS cells are treated *in vitro* or *in vivo* with trabectedin, FUS/CHOP is displaced from DNA leading to FUS/CHOP transcriptional inhibition (110, 126). The trabectedin-mediated inhibition of FUS/CHOP resulted in terminal differentiation of tumor cells into adipocytes. Identification of a therapy that causes a differentiation phenotype is important because patient survival for tumor types that are treated with differentiation agents can be over 95% (127). Additionally, differentiation agents generally possess fewer cytotoxic, off-target effects. While response rates to trabectedin in MLS patients have not achieved 100%, trabectedin has progressed through Phase III clinical trials and is now approved for MLS patients who have failed conventional chemotherapy (111).

Trabectedin has demonstrated efficacy in Ewing sarcoma patients and cell lines at concentrations similar to what was observed in MLS (112). Data from our lab first connected the anti-proliferative effect of trabectedin in Ewing sarcoma cells to inhibition of EWS/FLI1 activity (84). We established that trabectedin blocked EWS/FLI1 activity at the promoter of an important downstream target gene of EWS/FLI1 and that the inhibition correlated with decreased mRNA expression. EWS/FLI1 activity could also be inhibited in a fibrosarcoma cell line with forced EWS/FLI1 expression, which argues for specificity. In addition, we demonstrated that the inhibition of EWS/FLI1 correlated with

the generation of DNA damage as measured by the presence of histone H2AX phosphorylation. Unfortunately, these initial experiments did not identify the mechanism of EWS/FLI1 inhibition.

The goal of this study was to elucidate the mechanism of EWS/FLI1 inhibition in response to trabectedin at clinically relevant concentrations. By identifying a specific mechanism of action, we will gain insight into the biology of EWS/FLI1 that we can use to maximize suppression. In addition, there are over 20 tumor types that are defined by oncogenic transcription factors containing the N-terminal portion of a FET family member protein, many of which are sensitive to trabectedin (128). Therefore, the mechanism of action identified in Ewing sarcoma cells may be applicable to a much larger population of pediatric patients.

Results and Discussion

In order to elucidate the mechanism of trabectedin-mediated EWS/FLI1 inhibition, we identified the concentration and duration of trabectedin treatment that led to maximal EWS/FLI1 activity inhibition. The system that our laboratory developed to measure EWS/FLI1 activity is a cell-based assay using a well-known EWS/FLI1 binding site found in the NR0B1 promoter linked to a luminescent luciferase gene (NR0B1-Luc). In Ewing sarcoma cells, EWS/FLI1 can bind to the NR0B1 promoter sequence and drive expression of luciferase that can be directly measured by detecting luminescence (84). In parallel, we measure a cytomegalovirus-driven (CMV) luciferase construct whose expression is not influenced by EWS/FLI1 expression to ensure that the off-target effect of generalized transcription inhibition is not occurring (CMV-Luc). Finally, we perform

cell viability assays under the same conditions as the luciferase experiments to guarantee that any decrease in luciferase signal is not a consequence of cell death.

We treated the NR0B1-Luc and CMV-Luc cells at various concentrations of trabectedin for 8 hours and observed optimal EWS/FLI1 suppression with 5 nM trabectedin treatment (Figure 3A, black). At this specific time and concentration, there was no effect on the constitutively active CMV luciferase construct (Figure 3A, gray). In addition, no effects on cell viability were observed at this early time point (Data not shown). The inhibition of EWS/FLI1 activity observed in the luciferase experiments could be explained by a loss of EWS/FLI1 expression detected by qRT-PCR. For these experiments, we chose a time point that was prior to optimal suppression of luciferase because if the effect on activity is dominated by a change in expression, then EWS/FLI1 expression should change before the observed decrease in luciferase. To test this theory we treated Ewing sarcoma cells with 5 nM trabectedin for 6 hours and found that mRNA expression of EWS/FLI1 is suppressed (Figure 3B).

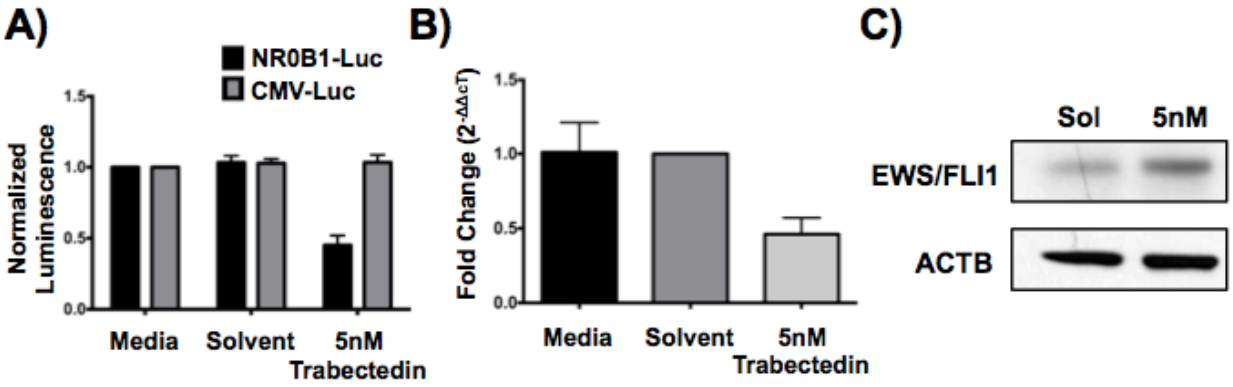

Figure 3: EWS/FLI1 activity and expression following trabectedin treatment. A) TC32 cells expressing either an EWS/FLI1-driven luciferase construct, NR0B1-Luc, or a constitutively driven luciferase construct, CMV-Luc, were treated with 5nM trabectedin for 8 hours. EWS/FLI1 activity and general transcription inhibition were detected by luminescence. B) TC32 cells were treated with 5nM trabectedin for 6 hours and EWS/FLI1 mRNA expression was detected by qRT-PCR. C) TC32 cells were treated with 5nM trabectedin for 18 hours and EWS/FLI1 protein expression was detected by western blotting.

Logically, the next experiment was to confirm that the inhibition of EWS/FLI1 activity by luciferase assay and mRNA expression by qRT-PCR extended to the protein level by performing a western blot. Because EWS/FLI1 protein has a longer half-life than EWS/FLI1 mRNA, we treated Ewing sarcoma cells with 5 nM trabectedin for a longer period of time before interrogating the change in protein expression. We treated the cells with 5 nM trabectedin for 18 hours, which is long enough to observe EWS/FLI1 target protein expression changes but short enough to avoid wide-scale apoptosis. Surprisingly, the expression of EWS/FLI1 protein is not affected by treatment with trabectedin (Figure 3C). These results suggest the mechanism of EWS/FLI1 inhibition is not a result of elimination of EWS/FLI1 expression from Ewing sarcoma cells.

Contrary to a decrease in expression after trabectedin treatment, the protein band for EWS/FLI1 appears to be more intense and slightly shifted. This implies that the protein is post-translationally modified upon drug treatment, which could explain the disconnect between the decrease in EWS/FLI1 mRNA expression and unaltered EWS/FLI1 protein expression.

Numerous EWS/FLI1 post-translational modifications have been characterized, which are thought to effect transactivation potential, protein-protein interactions, and stability of the fusion protein (129-132). Due to the shift of the EWS/FLI1 band upon drug treatment, we set out to confirm the presence and identity of a trabectedin-induced post-translational modification (PTM) by mass spectrometry. In order to obtain high quality mass spectrometry data, we optimized an immunoprecipitation (IP) protocol to purify endogenous EWS/FLI1 out of the TC32 cell line. To verify that the IP protocol worked, we ran a portion of the eluted protein on a poly-acrylamide gel (Figure 4, left).

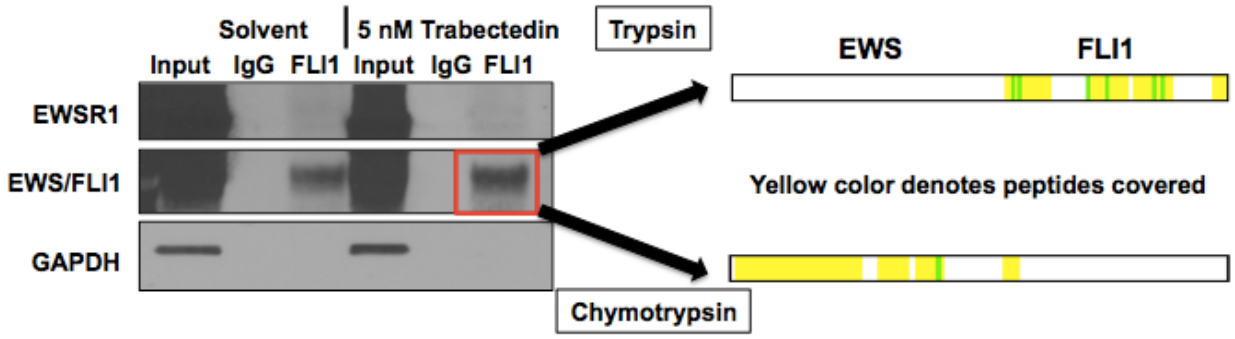

Figure 4: EWS/FLI1 immunoprecipitation and representative mass spectrometry analysis. Representative western blot demonstrates EWS/FLI1 immunoprecipitation using a FLI1 antibody. Red box indicates area of polyacrylamide gel that was cut out for mass spectrometry analysis. Following trypsin digest, FLI1 peptides were recovered and following chymotrypsin digest the EWS portion of the protein was identified. Yellow color denotes peptides recovered.

Upon achieving conditions most advantageous for EWS/FLI1 immunoprecipitation, samples were submitted to the Vanderbilt mass spectrometry core for analysis.

Our initial attempts to identify PTMs by mass spectrometry were unfavorably biased by the use of trypsin in the digestion protocol. Trypsin is a protease that enzymatically cleaves peptides immediately following a lysine or arginine residue (133). While the FLI1 portion of EWS/FLI1 contains a multitude of these residues, the EWSR1 portion contains only 1 of each residue. This limitation forced us to digest the proteins using chymotrypsin, a protease that cleaves at more sites (134). Because chymotrypsin cleaves the protein at more sites yielding smaller peptides, we dramatically increased the amount of protein that we used for these experiments to achieve adequate EWS/FLI1 coverage. The change to chymotrypsin led to much better coverage of the EWSR1 portion of EWS/FLI1, however the assay was not robust enough to identify a drug-induced PTM.

We did identify a phosphorylation event at Ser293 of EWS/FLI1 that corresponds to Ser241 of FLI1. This phosphorylation modification has been previously identified, but

not characterized, on FLI1 (135). Additionally, the phosphorylation of Ser293 is present in the control and trabectedin treated samples, so this PTM is unlikely to be related to drug treatment (Figure 4, right). Overall, we obtained high quality peptide reads on both the EWSR1 portion with chymotrypsin and the FLI1 portion with trypsin, but neither approach identified a PTM that was induced by trabectedin treatment.

Another method that we used to identify the mechanism of action for trabectedin in Ewing sarcoma cells was to examine the genetic response of Ewing sarcoma cells to trabectedin at a gene signature level. We have previously shown that low nanomolar trabectedin treatment generates DNA damage and suppresses EWS/FLI1 activity without affecting global transcription (84). Paradoxically, this defines trabectedin as both a general cytotoxic drug and a molecularly targeted therapy (124). However, it is possible that the DNA damage induced by trabectedin treatment activates a cellular response that specifically poisons EWS/FLI1-mediated transcription.

We examined previously published gene set enrichment analysis data from our laboratory to identify the genetic signatures that were activated following trabectedin treatment (84). We found Ewing sarcoma cells transcriptionally respond to trabectedin treatment in an identical manner that human embryonic kidney (HEK) cells respond to ultraviolet (UV) light treatment. This was perplexing because we believed the EWS/FLI1 protein mediates the sensitivity of Ewing sarcoma cells to trabectedin, and HEK cells do not the express the EWS/FLI1 protein. However, HEK cells express wild-type EWSR1 protein, which is ubiquitously expressed across most tissue types. Potentially, there is an inherent response of wild-type EWSR1 to UV light that is maintained in the EWS/FLI1 fusion protein's response to trabectedin treatment.

While the exact functions of EWSR1 have not been elucidated, it is known to bind DNA and RNA, and it is important for proper transcriptional regulation, DNA damage repair, and RNA processing (136). These functions of EWSR1 require its localization in the nucleus, and improper localization of EWSR1 to the cytoplasm has been shown to alter the transcriptional landscape in cells (137, 138). EWSR1 can also re-localize in the nucleus to the nucleolus leading to loss of binding at target sequences and widespread changes in mRNA processing at the level of splicing (139). The reported nucleolar enrichment of EWSR1 protein was specifically observed after UV light treatment of HEK cells.

We hypothesize the UV light induced re-localization of EWSR1 protein observed in HEK cells is maintained in Ewing sarcoma cells upon trabectedin treatment, which causes complete EWS/FLI1 inactivation. This phenomenon would explain the loss of EWS/FLI1 activity we have previously observed, even in the absence of a change in EWS/FLI1 protein expression. Both wild type EWSR1 and EWS/FLI1 proteins should re-localize to the nucleolus and become inactive; however, because EWSR1 is a member of the FET family of proteins, there are two other proteins that could compensate for the loss of EWSR1 activity. Additionally, normal cells are not dependent on EWSR1 function for cell survival and Ewing sarcoma cells absolutely depend on EWS/FLI1 activity, so this mechanism would explain the selectivity of the effect of trabectedin on Ewing sarcoma cells.

To investigate the localization of EWS/FLI1 in response to trabectedin treatment, we performed confocal microscopy experiments using a HA-tagged version of EWS/FLI1 (Figure 5). We treated cells with 5 nM trabectedin for 6 hours, and stained

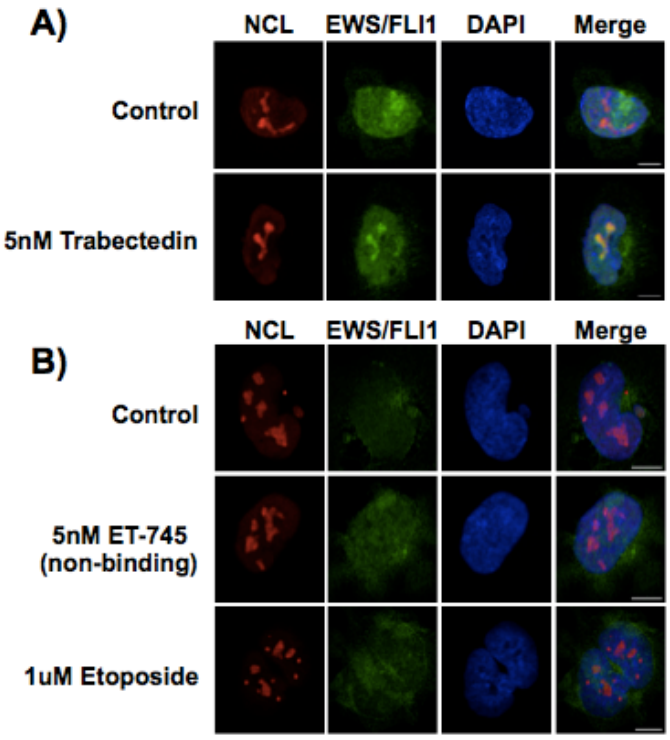

Figure 5: EWS/FLI1 re-localizes upon trabectedin treatment. A) Single-cell confocal microscopy demonstrates the effect of 5nM trabectedin on the localization of EWS/FLI1 after 6 hours of treatment in TC32 cells expressing an HA-tagged version of EWS/FLI1. Red, NCL (nucleolar marker). Green, HA-tagged EWS/FLI1. Blue, DAPI (DNA marker). B) Single-cell confocal microscopy of TC32 cells expressing an HA-tagged version of EWS/FLI1 treated with a non-binding trabectedin analog, ET-745, or high concentration of etoposide for 6 hours.

the cells with a HA-tag antibody. Because the initial report of EWSR1 re-localization observed enrichment in the nucleolus, we co-stained with an antibody for Nucleolin (NCL), an established marker for nucleolar structures (Figure 5A). After 6 hours, we observed a dramatic re-distribution of EWS/FLI1 in the nucleus following trabectedin treatment. This effect was not due to the presence of the HA-tag because we observed nucleolar enrichment with a FLI1 antibody as well (Data not shown). The kinetics of EWS/FLI1 re-localization was similar to the reported re-localization of wild-type EWSR1 protein in HEK cells in response to UV light. This implies that the two re-localization phenotypes are driven by the same mechanism.

We also confirmed the re-localization is dependent upon trabectedin binding to DNA. Treatment of Ewing sarcoma cells with a trabectedin analog that cannot bind DNA has no effect on EWS/FLI1 localization (Figure 5B). In addition, we confirmed the importance of the DNA damage response to EWS/FLI1 re-localization. Treatment of Ewing sarcoma cells with concentrations of trabectedin that do not induce DNA damage has no effect on EWS/FLI1 re-localization (Figure 5B). The re-localization phenotype is somewhat specific to the DNA damage response elicited by trabectedin because generalized DNA damage caused by high concentrations of other chemotherapeutic agents had no effect on EWS/FLI1 localization (Figure 5B).

In order to correlate the re-localization phenotype with a blockade of EWS/FLI1 activity, we first examined the ability of trabectedin to down-regulate a panel of well-characterized EWS/FLI1 target genes, ID2, NR0B1, RCOR1, and WRN at the mRNA level by qRT-PCR (Figure 6A). We demonstrated EWS/FLI1 target gene expression is suppressed in a dose-dependent manner when Ewing sarcoma cells are treated at trabectedin concentrations that re-localize EWS/FLI1 to the nucleolus. More importantly, when EWS/FLI1 activity is monitored at the protein level by western blot, target protein expression is suppressed (Figure 6B). Incubation of Ewing sarcoma cells with lower concentrations (<2.5 nM) of trabectedin has no effect on EWS/FLI1 localization or target protein expression (images not shown).

Finally, our hypothesis is predicated on the fact that the DNA damage generated by trabectedin elicits a cellular signal that leads to EWS/FLI1 re-localization and ultimately transcription factor inhibition. For this hypothesis to be valid, we needed to

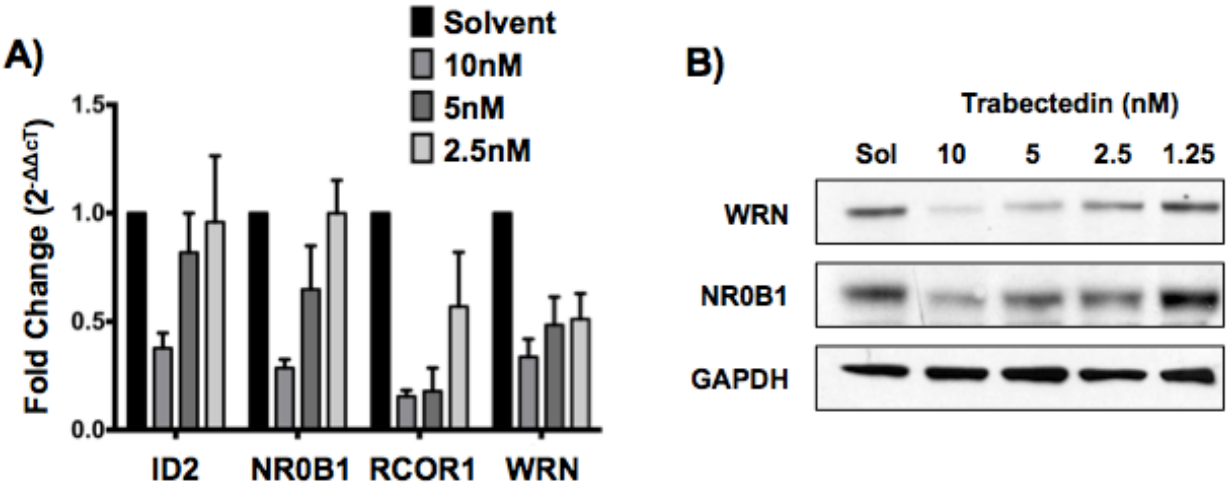

Figure 6: Re-localization phenotype correlates with EWS/FLI1 activity inhibition. A) TC32 cells were treated with the indicated concentration of trabectedin for 6 hours and EWS/FLI1 target gene mRNA expression was assayed by qRT-PCR. Fold change values are normalized to the housekeeping gene, GAPDH, whose expression is unaffected by trabectedin treatment. B) TC32 cells were incubated in the indicated concentration of trabectedin for 18 hours and EWS/FLI1 target gene protein expression was assayed by western blot. GAPDH is used as a loading control. Sol, solvent.

demonstrate that DNA damage is generated under similar treatments that lead to EWS/FLI1 re-localization. A well-known and reliable marker of trabectedin-induced DNA damage is the presence of phosphorylated histone variant H2AX (γH2AX) (140). This post-translational modification is deposited at Ser139 and is thought to be important for the recruitment of DNA damage repair factors (141).

After incubation of Ewing sarcoma cells with 5 nM trabectedin, we observed a significant increase in γH2AX foci formation as visualized by confocal microscopy (Figure 7A). In agreement with this, the presence of γH2AX mark is more abundant at the protein level (Figure 7B). γH2AX expression was not detectable by confocal microscopy or western blot, when Ewing sarcoma cells were treated with ET-745, the non-binding structural analog of trabectedin (data not shown).

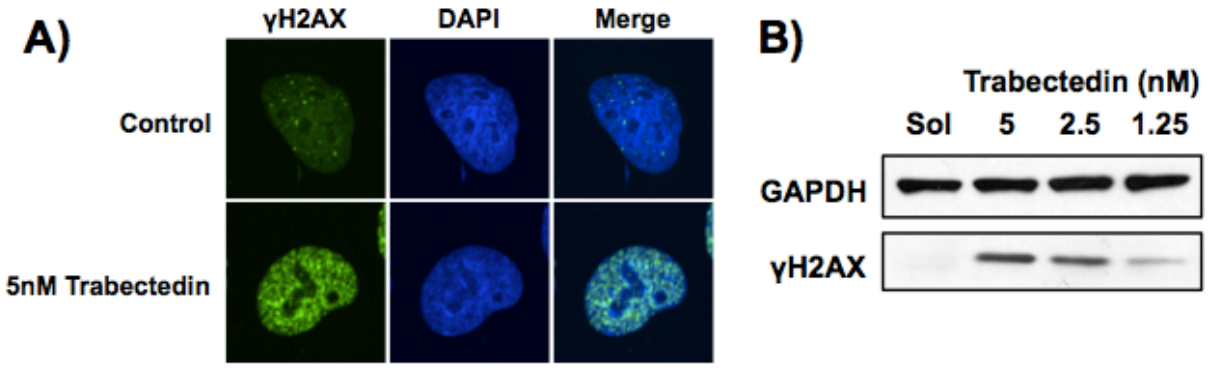

Figure 7: DNA damage is required for EWS/FLI1 inhibition. A) Single cell confocal microscopy of TC32 cells demonstrate γH2AX foci formation after 6 hours of treatment with 5nM trabectedin. Green, γH2AX (DNA damage marker); Blue, DAPI (DNA marker). B) TC32 cells were treated with the indicated concentration of trabectedin for 18 hours and the presence of DNA damage is detected by western blotting.

These data, coupled with the results of the luciferase experiments previously discussed, unequivocally establish trabectedin as a specific EWS/FLI1 inhibitor (Figures 3A, 5-7).

Conclusions

The results of these studies confirm the previously published trabectedin-mediated inhibition of EWS/FLI1 activity. We demonstrate EWS/FLI1 inhibition at the target gene promoter, mRNA, and protein levels. In addition, we establish the inhibition of EWS/FLI1 activity is not a result of protein loss, but instead depends on altered EWS/FLI1 localization in the nucleus. We believe this is an inherent stress response of the N-terminal portion of the wild-type EWSR1 protein domain that remains in the EWS/FLI1 fusion protein after translocation. In addition, we show the specific DNA damage induced by trabectedin is required to elicit the re-localization phenotype.

While wild-type EWSR1 re-localization is likely to occur in all cell types after trabectedin treatment, it has not been shown that inhibition of EWSR1 activity is

essential for cell viability in any cell type. This is probably due to the ubiquitous presence of other FET protein family members, FUS and TAF15, which function somewhat redundantly to EWSR1. Importantly, this provides rationale for the selectivity of Ewing sarcoma cells to the effects of trabectedin because Ewing sarcoma cells absolutely depend on the constitutive activity of EWS/FLI1 for cell survival.

The immediate implications for this mechanism are substantial. The re-localization phenotype provides a mechanism-based output to identify other EWS/FLI1 inhibitors in a high-throughput fashion. In addition to trabectedin, we currently have a library of over 80 structural analogs of trabectedin that can now be rapidly screened for inhibition of EWS/FLI1 activity using microscopy. We can also re-examine previously identified EWS/FLI1 inhibitors to investigate whether this re-localization mechanism is specific to trabectedin or more widely applicable.

More importantly, the re-localization of EWS/FLI1 may be used in the clinic as an endpoint to determine whether a therapeutic regimen is having an on-target effect. Because ES patients are not completely homogeneous, drug activity may be slightly altered from patient to patient. However, by examining the localization of EWS/FLI1 following treatment, optimizing the activity of trabectedin by alterations in drug scheduling has the potential to become a reality.

Chapter 3

Optimizing the Schedule of Administration of Trabectedin

Introduction

The purpose of this chapter is to determine the most effective approach to use trabectedin to suppress EWS/FLI1 activity in vivo and in patients. Now that we have characterized the mechanism of EWS/FLI1 suppression and determined that it occurred at clinically relevant concentrations of drug, we will optimize the exposure of Ewing sarcoma cells to trabectedin treatment. More precisely, we will model the exposure of Ewing sarcoma cells to trabectedin, administered as a 1-, 3- or 24-hour infusion. We will correlate these exposures with the loss of cell viability *in vitro*, induction of the re-localization of EWS/FLI1, and examine the potential mechanism of sustained suppression of EWS/FLI1 activity. Ultimately, these data will be used to guide future clinical trial design.

We have shown that Ewing sarcoma cells are particularly sensitive to trabectedin treatment. In the previous chapter, we linked this selectivity to trabectedin to the re-localization of EWS/FLI1 protein and suppression of its activity. Because almost all Ewing sarcoma patients have EWS/FLI1, whose activity is required for tumor cell viability, we believe the trabectedin-induced suppression of EWS/FLI1 should translate in high response rates. However, the response of Ewing sarcoma patients to trabectedin therapy during clinical testing has not been consistent. With the mechanism of action elucidated, we can now model the achieved clinical exposures *in vitro* and model the optimal schedule of administration of trabectedin in Ewing sarcoma patients.

The schedule of administration for a particular chemotherapy is a critical aspect of drug activity. Optimal dosing and duration of treatment must be worked out in clinical trials in order to mitigate off-target effects while maximizing clinical benefit. It has been demonstrated that optimization of drug schedule can alter the observed dose limiting toxicities and positively affect response rates (142-144). For example, it was found in multiple clinical trials that the topoisomerase II inhibitor, etoposide, displays improved activity when total exposure is increased by administering a low dose of drug for a prolonged period of time (144, 145). This protracted schedule of administration significantly increased response rates. In contrast, other chemotherapies such as teniposide (VM-26) only demonstrated enhanced clinical activity after achieving a threshold concentration (12 mg/L) in patients (146).

The schedule of administration of trabectedin has not been optimized for Ewing sarcoma patients. Trabectedin has completed Phase I and II clinical testing in pediatric cohorts containing Ewing sarcoma patients (112, 113). While the Phase I trial was only designed to evaluate the safety of trabectedin, clinical responses were also noted. Importantly, two out of three treatment-refractory Ewing sarcoma patients achieved a clinical response to single-agent trabectedin therapy. Following this schedule of administration, a durable and complete response was observed in a Ewing sarcoma patient with widely metastatic disease. This clinical trial administered trabectedin at doses of either 1.1 or 1.3 mg/m^2 as a 3-hour infusion. With this schedule, patients achieved a maximum serum concentration (C_{max}) of trabectedin of approximately 14 nM (112). The concentration of trabectedin in serum decreased rapidly following the infusion and led to reversible and non-cumulative toxicities.

An additional Phase I trial was performed to study the safety profile and pharmacokinetics of trabectedin administered as a 1–hour infusion every week for 3 weeks (147). No Ewing sarcoma patients were enrolled in this trial, but several soft tissue sarcoma patients demonstrated partial response or stable disease. The maximum tolerated dose was identified as 0.61 mg/m^2 and led to serum concentrations above 15 nM.

Based on these positive Phase I clinical trial results, trabectedin entered Phase II clinical testing (113). Drawing on observations from adult clinical trials, the schedule of administration for the phase II trial in Ewing sarcoma was adjusted from a 3-hour infusion to a 24-hour infusion. In this trial the dose of trabectedin was only slightly increased to 1.5 mg/m^2, which led to trabectedin serum concentrations (C_{max}) that were significantly lower (approximately 3 nM) than the Phase I trials. While this schedule of administration increased the overall exposure to trabectedin, only 1/10 Ewing sarcoma patients enrolled demonstrated stable disease. For this reason, trabectedin as a single agent did not show sufficient activity for continued clinical development in Ewing sarcoma. In agreement, we have demonstrated that EWS/FLI1 inhibition is negligible when Ewing sarcoma cells are treated with trabectedin at concentrations achieved in the Phase II trial (84).

It is likely that the adjusted schedule of administration in the Phase II trial negatively affected the outcome by limiting the concentration of drug that reached the tumor cells. We believe, unlike other sarcoma subtypes that are responsive to trabectedin, the on-target effect in Ewing sarcoma is mediated by C_{max} and not increased exposure (111). In agreement with this hypothesis, Beumer et al.

demonstrated that trabectedin administered as a 3-hour or 24-hour infusion obtained similar exposure levels as measured by total area under the curve (AUC) (148). The single parameter that varied significantly between the two schedules was C_{max}, which was consistently higher following the 3-hour infusion relative to the 24-hour infusion.

The goal of this study is to use the re-localization of EWS/FLI1 to investigate the effect of C_{max} and exposure to trabectedin on Ewing sarcoma cells. We will show that the optimal suppression of EWS/FLI1 is dependent upon achieving a threshold C_{max} that is more similar to the Phase I clinical trials. The cell culture models developed in these studies will help guide further clinical trial design and will provide insight into the disparate conclusions of the Phase I and II clinical trials.

Results and Discussion

In order to model the effects of C_{max} versus exposure, we adjusted our cell culture models to mirror the pharmacokinetic data obtained from patients in the two clinical studies. To model the Phase I clinical trials, we treated Ewing sarcoma cells with high concentrations of trabectedin for a short amount of time followed by replacement with regular culture media. Using this model, we found that the half-life of the drug in cells is approximately 4 hours (Data not shown). To model the Phase II clinical trial, we treated Ewing sarcoma cells with a low dose of trabectedin for longer periods of time without replacing the culture media. Using this cell culture model, we can test numerous variables, including total exposure, concentration, or duration of treatment, and determine which factor maximizes the inhibition of EWS/FLI1.

The first factor that we examined was total exposure. We incubated Ewing sarcoma cells with equivalent exposures of trabectedin at various concentrations.

Exposure in these experiments is defined as the concentration of drug multiplied by the duration of treatment and is measured in units of nM*min. We observed the cellular response by measuring the growth inhibition in real time using time-lapse microscopy. We have demonstrated that Ewing sarcoma cells respond to the same exposure of trabectedin differentially (Figure 8A). We showed that 10 nM treatment for 1-hour (600 nM*min) resulted in a 75% decrease in cell growth, but 5 nM trabectedin for 2-hours (600 nM*min) demonstrated only a partial delay in growth kinetics. This data argues that the effect on Ewing sarcoma cell growth is not dependent on exposure, but is dependent on achieving a threshold concentration.

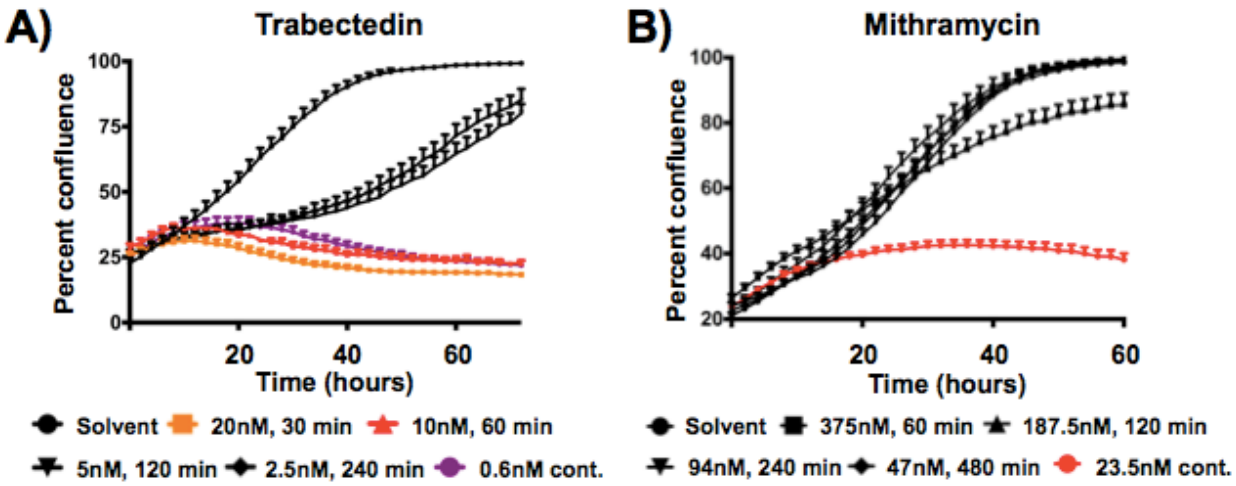

Figure 8: Activity of trabectedin in Ewing sarcoma is not dependent upon exposure. A) TC32 cells were equally exposed to 600nM*min trabectedin at the indicated concentration followed by washout with regular media. Confluence was measured in real time by phase contrast microscopy. Continuous treatment with 20nM trabectedin is used as a positive control. B) TC32 cells were equally exposed to 22,500nM*min mithramycin at the indicated concentration followed by washout with regular media. 23.5nM mithramycin is used as a positive control. Confluence was measured in real time by phase contrast microscopy.

In addition to trabectedin, we also tested the C_{max} effect of mithramycin, an EWS/FLI1 inhibitor whose mechanism of inhibition has yet to be elucidated. We treated Ewing sarcoma cells with equivalent exposures (22,500 nM*min) to mithramycin at

various concentrations. Even when treated with physiologically irrelevant exposures to mithramycin, we observed no effect on Ewing sarcoma cell growth at any concentration tested (Figure 8B). On the contrary, we observed a significant effect on cell growth when mithramycin was administered continuously at a lower concentration (Data not shown).

To test the effect of C_{max} on Ewing sarcoma cell growth, we performed a classic pharmacology assay that is used to test the schedule dependency of drugs (149). To demonstrate the schedule-dependency of trabectedin, we analyzed the cytotoxicity of trabectedin at many concentrations and durations of treatment. This data is represented by plotting the effect of drug treatment (y-axis) as a function of total drug exposure (x-axis) (149). This type of graph allows for the simultaneous measurement of effect across a wide range of exposures. In theory, this assay would be more meaningful performed *in vivo*; however, the solubility of trabectedin and effect of drug treatment on the health of the tail vein of the mouse forced us to perform this assay in cell culture. The assay described here is the currently accepted standard for establishing schedule-dependency using *in vitro* cell culture models (149).

To demonstrate schedule-dependency, we treated Ewing sarcoma cell lines with a wide variety of exposures to trabectedin followed by washout with regular cell culture medium. 48 hours after the initial drug treatment, cell number was measured by standard MTS assay. If the effect of trabectedin is dependent on schedule, then the exposure-effect curves should not overlap. We observed a schedule-dependent effect on growth of Ewing sarcoma cells following trabectedin treatment as shown by the leftward shift of the curves (Figure 9, left). The growth inhibitory effect seemed to be

dominated by the concentration of drug, which is supported by the fact that 25 nM trabectedin treatment resulted in the same phenotype whether the cells were treated for six minutes or 2,880 minutes. Additionally, these graphs imply that there is no added benefit of increasing exposure levels if an appropriate C_{max} is achieved.

As a control to ensure that the schedule-dependency was not a generalized effect of treatment with drugs that bind DNA in the minor groove, we treated Ewing sarcoma cells with mithramycin in a similar fashion as the previous trabectedin exposure experiments. The mithramycin experiments were carried out at much higher exposures as indicated on the x-axis in Figure 9. We observed no schedule-dependent effect following treatment of Ewing sarcoma cells with low exposures of mithramycin (Figure 9, right). We did observe shifts in exposure curves for mithramycin treatments longer than eight hours; however, the concentration of drug required to establish these exposures exceed concentrations that are achievable in patients by 20X.

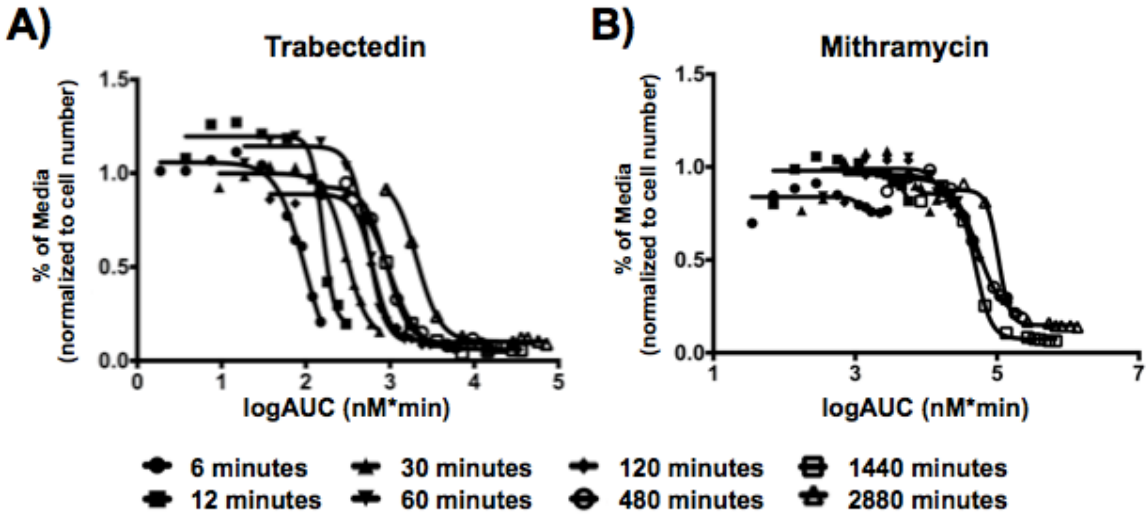

Figure 9: Effect of trabectedin on cell viability is schedule-dependent. A) TC32 cells were treated at various concentrations of trabectedin for the indicated duration of time. Following treatment, drug was washed out and fresh drug-free media was added. After 48 hours, MTS assays were performed and viability was graphed as a function of exposure. B) Same as A, except mithramycin was used in place of trabectedin.

In order to correlate the growth inhibitory effect of C_{max} with EWS/FLI1 inhibition, we investigated the effect of transient trabectedin treatment in our previously described luciferase system. By using a luciferase construct fused downstream of a well-known EWS/FLI1-driven promoter (NR0B1-luc), we identified maximum EWS/FLI1 inhibition and an absence of general transcriptional inhibition with conditions that reflect the Phase I clinical trial (Figure 10A, black bars). We show that transient treatment of Ewing sarcoma cells with trabectedin (24 nM for 1-hour) demonstrates improved inhibition of EWS/FLI1 when compared to continuous, 8-hour treatment with 5 nM trabectedin (transient inhibition = 54% of control; continuous inhibition = 39% of control) (Figure 10A). Importantly, patients only achieved 3 nM trabectedin in serum in the Phase II trial, which under continuous treatment leads to a negligible effect on EWS/FLI1 activity (84). In addition, general transcription inhibition and cell viability were not affected at the highest concentration of drug washout (Figure 10A, gray bars and data not shown). These data suggest that the C_{max} effect of trabectedin is on-target and leads to the inhibition of EWS/FLI1 activity.

To verify that the inhibition of EWS/FLI1 observed at the promoter level is maintained at the protein level, we examined expression of the EWS/FLI1 down-stream target, NR0B1. We showed a suppression of NR0B1 in a panel of Ewing sarcoma cell lines following treatment with conditions modeling the high C_{max}, similar to the Phase I clinical trial (Figure 10B, C_{max} high). There is no effect on NR0B1 protein expression with the low dose, continuous cell culture model that is more representative of the Phase II clinical trial (Figure 10B, C_{max} low). These experiments were performed with

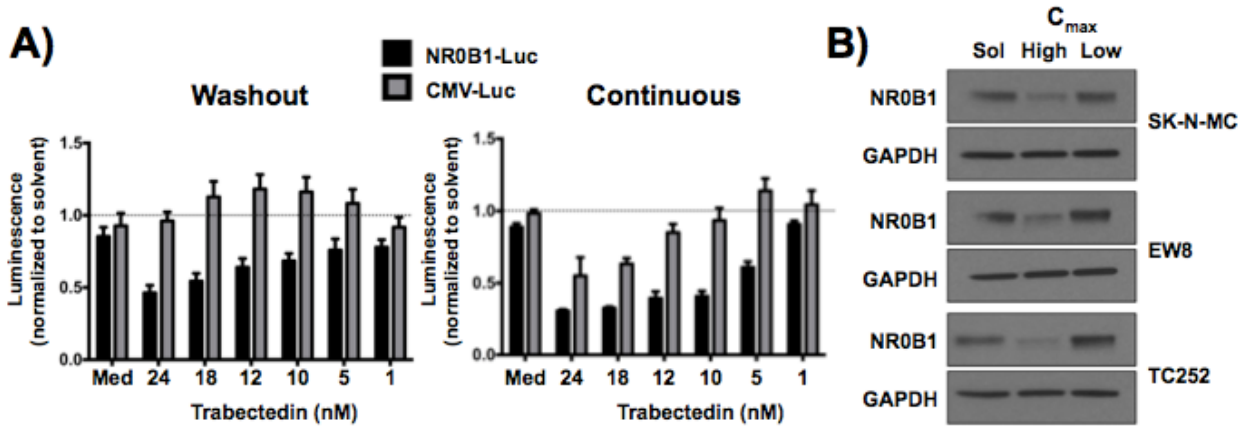

Figure 10: High C_{max} treatment inhibits EWS/FLI1 activity and NR0B1 expression. TC32 cells expressing either an EWS/FLI1-driven luciferase construct, NR0B1-Luc, or a constitutively driven luciferase construct, CMV-Luc, were treated with the indicated concentration of trabectedin for 1 hour followed by regular media(left) or continuously (right). EWS/FLI1 activity and general transcription inhibition were detected by luminescence. B) NR0B1 protein expression is suppressed following washout treatment with high concentration trabectedin. SK-N-MC, EW8, or TC252 cells were treated for 1 hour with 24nM trabectedin (C_{max} high) or 1nM trabectedin for 24 hours continuously (C_{max} low). Sol, Solvent.

equivalent exposures (1440 nM*min) and again suggest that the inhibitory effect on EWS/FLI1 activity is driven by treatment with higher concentrations of trabectedin.

The schedule-dependency of trabectedin, but not mithramycin is likely linked to their respective mechanisms of action in Ewing sarcoma cells. The mechanism of EWS/FLI1 inhibition in response to mithramycin treatment is an ongoing area of research, but we know mithramycin does not induce re-distribution of EWS/FLI1 at any concentration (Data not shown). We previously linked the on-target suppression of EWS/FLI1 activity to the re-distribution of EWS/FLI1 following trabectedin treatment. These experiments were carried out under continuous drug treatment and do not reflect the clinical setting.

Because of the sustained delay in cell growth observed following transient trabectedin treatment, we hypothesized that the effect was on-target. This means that the re-localization phenomenon should occur following short-term trabectedin treatment. Therefore, we treated Ewing sarcoma cells that stably express a HA-tagged version of

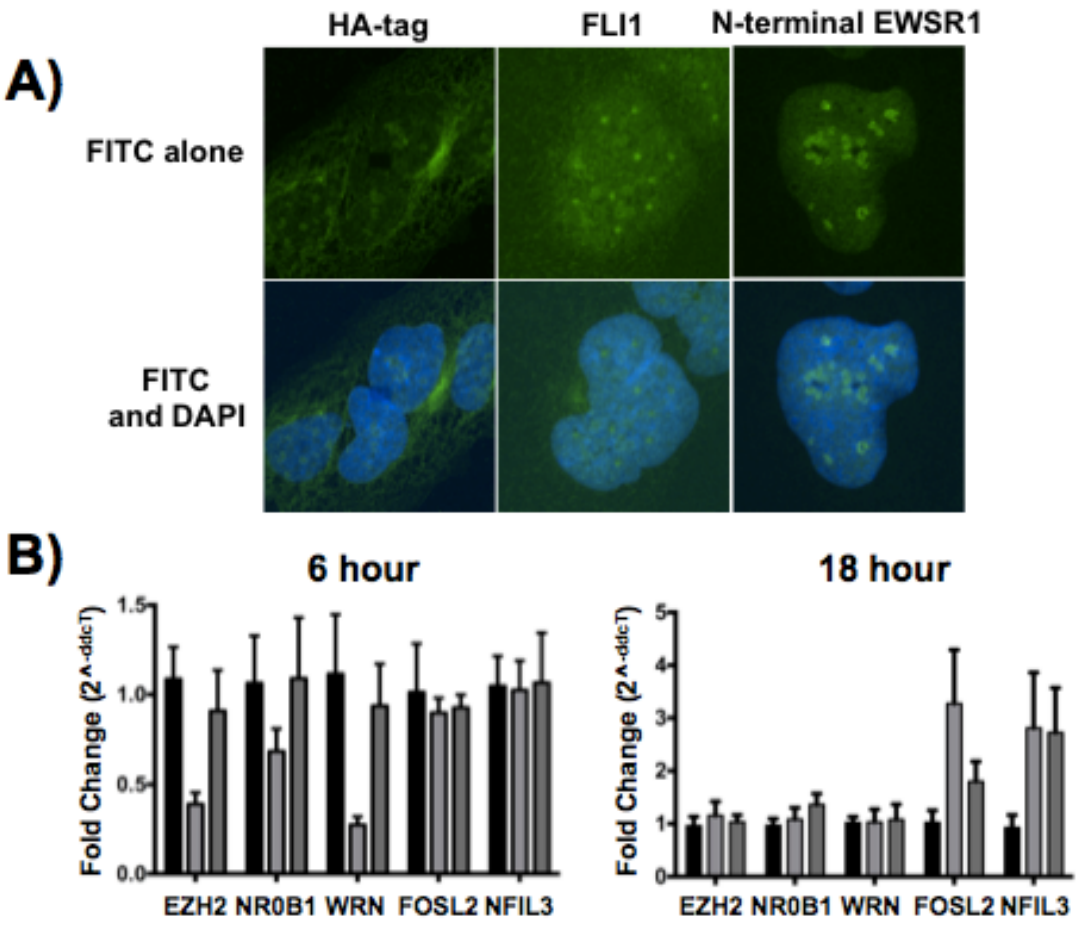

Figure 11: High C_{max} treatment re-localizes EWS/FLI1 and suppresses EWS/FLI1 target gene expression. A) Single cell confocal microscopy images showing the effect of 1-hour, 24 nM trabectedin treatment followed by 5 hours of drug-free culture media. B) qRT-PCR data demonstrating the effect of trabectedin at high (1-hour washout treatment) and low (low dose continuous treatment) C_{max} levels in A673 cells at 6-hours and 18-hours.

EWS/FLI1 were treated with trabectedin for 1-hour at which point the cell culture media was replaced with standard, drug free medium. By confocal microscopy, we observed EWS/FLI1 re-localization using HA-tag, FLI1, and EWSR1 antibodies (Figure 11A). The antigen used to make the EWSR1 antibody flanks the Gly174 residue and detects wild type EWSR1 and EWS/FLI1.

To further demonstrate an on-target effect driven by high C_{max} treatment, we examined the expression of EWS/FLI1 target genes at the mRNA level 6-hours and 18-hours after washout. At early time points that coincide with EWS/FLI1 re-localization the induced target genes of EWS/FLI1 (EZH2, NR0B1, and WRN) were all repressed; however, their expression recovers at the later, 18-hour time point (Figure 11B). Interestingly, there is no effect on repressed target genes (FOSL2 and NFIL3) of EWS/FLI1 at the 6-hour time point, but these genes are significantly induced at the later, 18-hour time point (Figure 11B). As previously mentioned, the repressed target genes of EWS/FLI1 have not been well characterized; therefore, FOSL2 and NFIL3 may represent indirectly repressed genes. The induction of gene expression following trabectedin treatment does argue against a general inhibition of transcription. Additionally, we demonstrated the suppression of EWS/FLI1 activity at the level of target protein expression. We treated a panel of Ewing sarcoma cell lines using our high C_{max} or low C_{max} model and examined the expression of EWS/FLI1 target proteins (Figure 12)

One possible explanation for the sustained suppression of EWS/FLI1 target proteins is that the re-localization of EWS/FLI1 occurs concomitantly with a local change in chromatin that blocks further protein expression. It is well known that EWS/FLI1 regulates the expression of important epigenetic readers, writers, and erasers, including EZH2 (see above data). EZH2 is an induced EWS/FLI1 target that is generally associated with the generation of H3K27me3 that leads to gene suppression (57). Because EZH2 expression is suppressed following trabectedin treatment, we do not

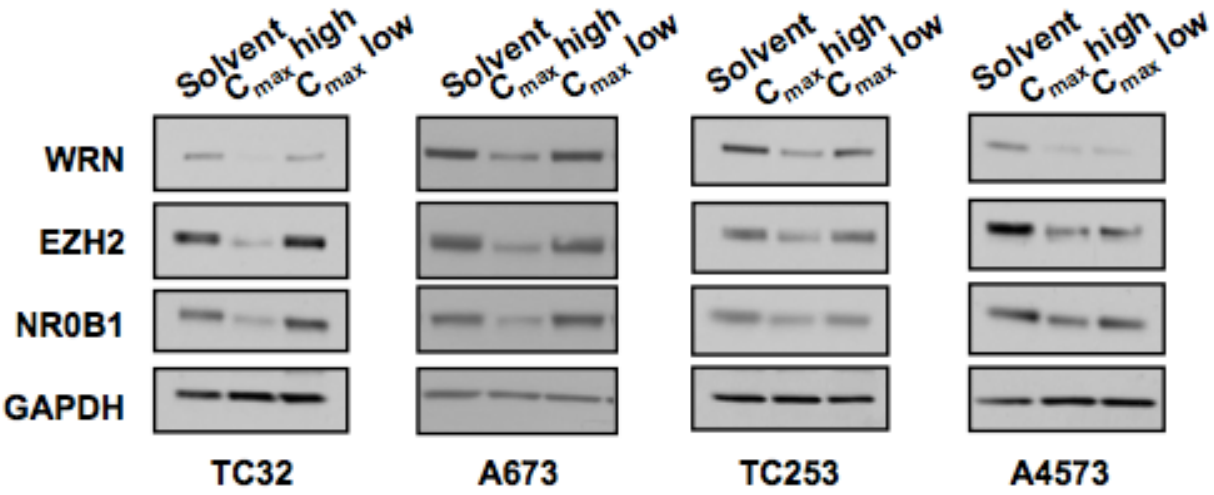

Figure 12: High C_{max} treatment suppresses EWS/FLI1 target protein expression. Ewing sarcoma cells were treated for 1-hour with equivalent exposures of trabectedin to model high and low C_{max} effects. High C_{max} for each cell line is as follows: TC32, 24 nM; A673, 18 nM; TC253 and A4573, 12 nM.

believe that the deposition of H3K27me3 is responsible for the sustained suppression of EWS/FLI1 activity.

Another critical epigenetic mark that is associated with transcriptional suppression is H3K9me3 (150). H3K9me3 has been identified as an important epigenetic modification in satellite DNA sequences, similar to sequences bound by EWS/FLI1 (151). In cells, H3K9me3 is recognized by HP1 protein, which recruits the SUV39H/SETDB proteins that catalyzes the formation of H3K9me3 (152). This cycle leads to the propagation of a large amount of H3K9me3 mark, which can be seen as foci using confocal microscopy. We showed a significant increase in HP1, SUV39H2, and the H3K9me3 mark using our high C_{max} model (Figure 13A). The up-regulation of HP1 and SUV39H2 proteins occur very early (within 1-hour) following treatment, and is followed by an increase in H3K9me3. The increase in H3K9me3 observed by western blot can also be seen using confocal microscopy (Figure 13B). The pattern of H3K9me3

foci formation appears to occur around the nucleolus, which matches the pattern of EWS/FLI1 localization following the same treatment conditions.

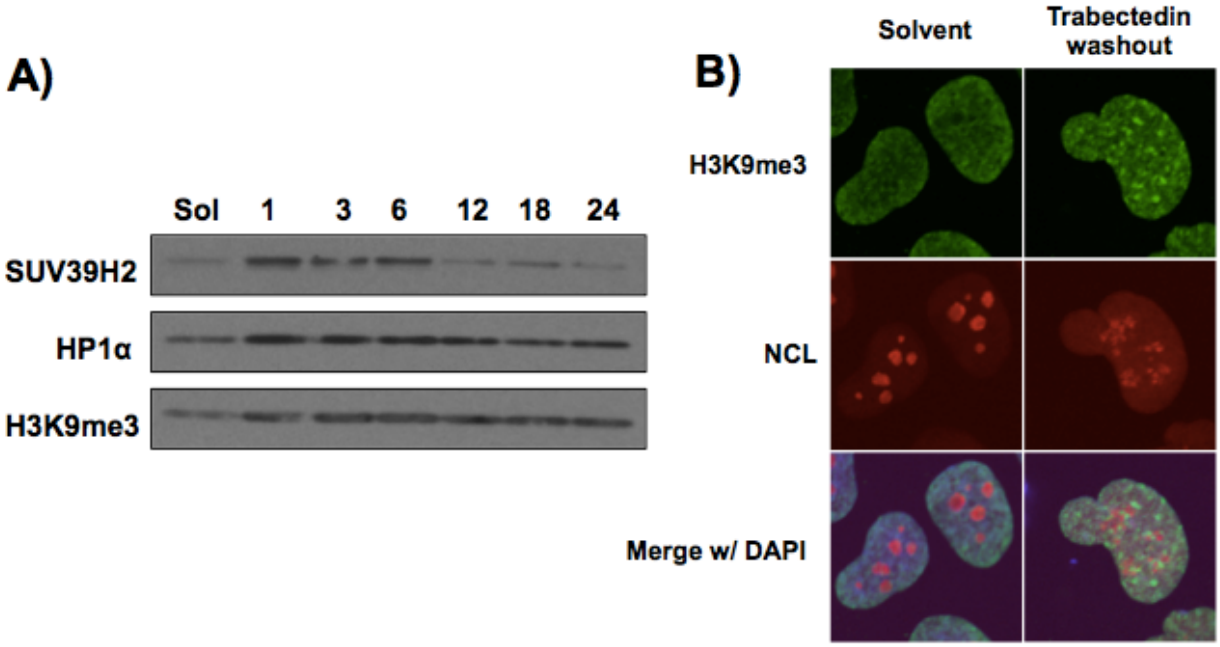

Figure 13: Trabectedin washout induces epigenetic alterations. A) The insoluble chromatin fraction from TC32 cells treated with trabectedin for 1-hour followed by incubation in regular media was collected at the indicated time point. Expression of proteins critical for the generation of H3K9me3 was examined by western blot. Sol, Solvent. B) Single cell imaging of Ewing sarcoma cells following 1-hour washout of trabectedin were imaged at 6 hours. Green = H3K9me3; Red = NCL (nucleolar marker); Blue = DAPI.

Conclusions

The results of these studies demonstrate the importance of optimizing the proper trabectedin schedule for Ewing sarcoma patients. We show that the on-target effect of trabectedin is not dependent on exposure to drug, and only occurs following transient treatment with high concentration of trabectedin. This schedule results in durable Ewing sarcoma cell growth inhibition *in vitro*, decreased EWS/FLI1 activity due to redistribution of the protein in the nucleus, and a change in expression of critical EWS/FLI1 target genes that we believe is mediated by an epigenetic switch. Conversely, we observe no

on-target effect of trabectedin when Ewing sarcoma cells are treated with low concentrations for prolonged periods of time.

An important conclusion that can be drawn from these studies is that *in vitro* schedule of administration optimization may be clinically beneficial. These studies can be performed in cell lines, and provide meaningful insight into the potential clinical benefit and mechanism of action particularly for a well-defined target such as EWS/FLI1. From these studies we have learned that, unlike other sarcoma subtypes, maximum exposure to trabectedin (defined by maximum AUC) does not define clinical activity in Ewing sarcoma which instead depends on a high Cmax (111).

Another clinically relevant observation that we have made from these experiments is the potential to identify subsets of patients that may be hypersensitive to trabectedin treatment. By screening a panel of Ewing sarcoma cell lines, we found that cell lines containing the variant Type III isoform of EWS/FLI1 respond to lower concentrations of trabectedin (Data not shown). This heightened sensitivity to trabectedin correlated with decreased EWS/FLI1 target protein expression *in vitro* and prolonged survival in two Ewing sarcoma xenografts. In agreement with an on-target effect of EWS/FLI1 inhibition in these xenografts, tumors appear to differentiate down various mesenchymal lineages (Data not shown). These data suggest that Ewing sarcoma patients should be sub-typed by qRT-PCR in the clinic to determine the variant isoform of EWS/FLI1 they express, which is currently not the standard.

While we have made numerous findings regarding the effect of C_{max} and schedule of administration, the mechanism of long-term EWS/FLI1 inhibition has not yet been fully elucidated. Our current working hypothesis is that the short term, high

concentration of trabectedin treatment re-localizes EWS/FLI1 to the nucleolus. While EWS/FLI1 is enriched in the nucleolus, we believe that H3K9me3 is deposited on repeat sequences leading to long-term gene silencing. H3K9me3 has previously been shown to mark tandem repeat DNA sequences similar to the sequences that EWS/FLI1 preferentially binds (153). In agreement with this hypothesis, we observe H3K9me3 foci around the nucleolus following transient trabectedin treatment. The formation of foci coincides with the accumulation of EWS/FLI1 in the nucleolus. It is likely that this apparent co-localization of EWS/FLI1 and H3K9me3 leads to sustained target gene suppression that triggers the cells to undergo apoptosis, senescence, or differentiation. We believe a majority of the cells eventually die, and the remaining cells differentiate down the mesenchymal lineage to form adipocytes or cartilage.

Finally, the high concentration of trabectedin used in these studies to model the C_{max} effect is slightly higher than the concentrations obtained in clinical trials. However, we needed to use these concentrations because all of the data shown here was performed as single agent studies. In the combination setting, we believe that clinically achievable concentrations of trabectedin can be used to obtain the same effect, which we have previously shown when trabectedin was combined with the topoisomerase I inhibitor, irinotecan (114, 154)

Chapter 4

Identifying a Trabectedin Analog with an Improved Therapeutic Window

Introduction

The goal of this study was to identify structural analogs of trabectedin that maintain EWS/FLI1 activity and improved pharmacokinetic qualities. This should expand the therapeutic window of treatment, lead to fewer off-target effects, and allow patients to achieve a higher C_{max}. Additionally, a small molecule that completely inhibits EWS/FLI1 activity should lead to a decrease in proliferative capacity and release the differentiation block of Ewing sarcoma cells causing the cells to differentiate down the mesenchymal lineage.

Our laboratory has previously shown that one way to circumvent the pitfalls of a narrow therapeutic window is to identify structural analogs of the parent compound that maintain the on-target effect at concentrations that can be safely achieved in patients (86). This report characterized the effect of two novel mithramycin analogs on EWS/FLI1 inhibition, EC-8105 and EC-8042. EC-8105 demonstrated increased potency and was found to maintain EWS/FLI1 inhibition when administered at lower concentrations than mithramycin. EC-8042 maintained EWS/FLI1 activity inhibition when administered at concentrations similar to mithramycin, but was identified to be much less toxic as the maximum tolerated dose in animal models was nearly 10-times that of mithramycin. This decrease in toxicity allowed a higher concentration of EC-8042 to be administered and these mice achieved a significantly higher C_{max}.

We believe this optimization strategy can also be utilized to expand the therapeutic window of trabectedin, which was limited in the Phase I clinical trial (112). In an effort to improve this window in the clinic, trabectedin was administered as a 24-hour infusion (113). It has been shown in certain sarcoma subtypes that a longer infusion of trabectedin is better tolerated and results in improved rates of progression free survival and overall survival (155). While this was effective in liposarcomas and leiomyosarcomas, the extended schedule of trabectedin in Ewing sarcoma patients demonstrated no clinical benefit (113). An alternative approach that we employed was to identify structural analogs of trabectedin with an improved therapeutic window.

While the antitumor effects of numerous structural analogs of trabectedin have been characterized *in vitro*, only zalypsis (PM00104) and lurbinectedin (PM01183) have advanced into the clinic for testing (96, 140, 156). Zalypsis is a member of the renieramycin family of compounds that contains a tetrahydroisoquinoline group (157). Similar to trabectedin, zalypsis has demonstrated *in vitro* antitumor activity in a wide variety of liquid and solid tumor cell lines at picomolar and low nanomolar concentrations (158, 159). The characterized mechanism of cytotoxicity for zalypsis is similar to trabectedin, however the binding properties and the nucleotide excision repair dependencies are slightly different (140). These differences in activity can be traced back to the structural variations between the two molecules.

The A and B rings are of trabectedin and zalypsis are identical, but the C-rings are very distinct (Figure 14, left). The C-ring of trabectedin is rigid, while the C-ring of zalypsis is much more flexible. The flexibility in the C-ring of zalypsis does not affect activity *in vitro*, however it seems to negatively affect the antitumor activity in patients.

To date, zalypsis has not displayed any activity in clinical testing including a Phase II trial in Ewing sarcoma, likely due to the flexibility of the C-ring (160, 161). The defined C-ring of trabectedin is thought to interact with and inhibit the function of specific proteins, and thus the flexibility of the C-ring of zalypsis may actually inhibit its utility in the clinic. This observation underscores the fundamental contribution of the C-ring structure of trabectedin to antitumor activity, and implies DNA binding coordinated through the A and B rings is not responsible for the on-target mechanism of action.

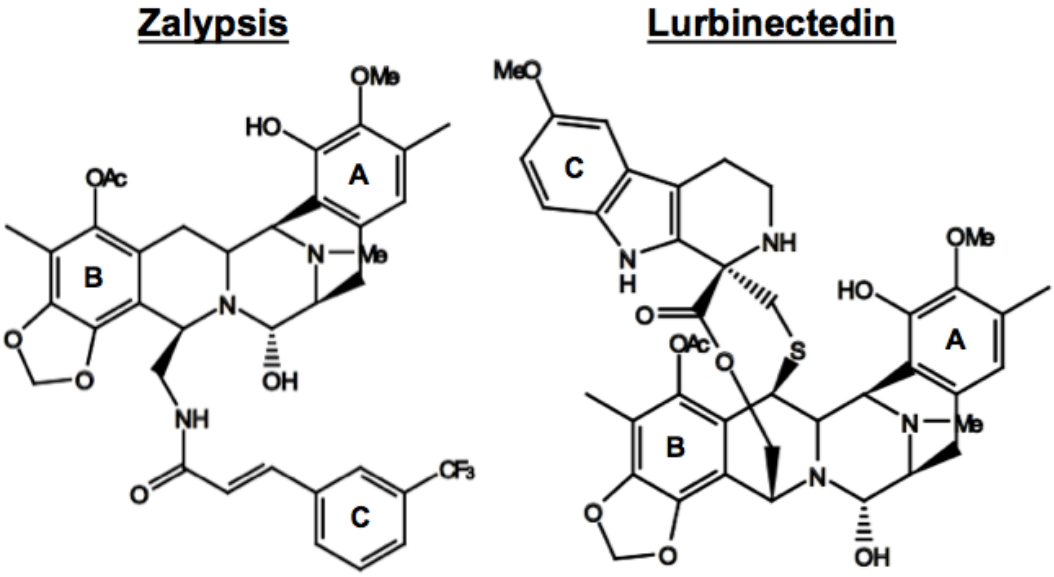

Figure 14: The structure of Zalypsis and Lurbinectedin. The structures of Zalypsis (PM00104) and Lurbinectedin (PM01183) are shown. The A, B, and C ring moieties are labeled.

As opposed to zalypsis, lurbinectedin, a closely related structural analog of trabectedin, has demonstrated activity in early phase clinical trials (162). Unlike zalypsis, lurbinectedin has a rigid C-ring moiety that differs slightly in structure from trabectedin (Figure 14, right) (156). Importantly, decreased toxicity was observed in Phase I clinical testing in patients with solid tumors as a single agent and in the combination setting (162, 163). Patients enrolled in the dose-escalation trial were able

to be administered over three times the dose of trabectedin before reaching the maximum tolerated dose (162). Additionally, the recommended dose was administered as a 1-hour infusion leading to serum concentrations that were nearly 20-times higher than the C_{max} achieved in the negative Phase II trial of trabectedin (113). Included in the Phase I trial of lurbinectedin were two soft tissue sarcoma patients with synovial sarcoma, who both displayed tumor shrinkage and long-term progression free survival. This clinical trial data suggests that lurbinectedin may be active in other soft tissue sarcoma including Ewing sarcoma.

At the onset of these studies, the effect of lurbinectedin on EWS/FLI1 activity and Ewing sarcoma patients was unknown. The goal of this study was to determine if lurbinectedin is a more clinically relevant analog of trabectedin. By identifying a less toxic analog of trabectedin that maintains inhibition of EWS/FLI1 activity at similar concentrations, we will be able to expand the therapeutic window that limits the efficacy of trabectedin.

Results and Discussion

Due to the fact that lurbinectedin was found to be less toxic than trabectedin in clinical testing, we were surprised to observe almost identical effects on cell growth *in vitro*. Both drugs have picomolar GI50 values in Ewing sarcoma cells (Trabectedin GI50 = 350 pM; Lurbinectedin GI50 = 340 pM), and long-term treatment leads to Ewing sarcoma cell death (Data not shown).

Considering both trabectedin and lurbinectedin display nearly identical GI50 values, it is likely that both drugs work through a similar mechanism of action. In order to determine if lurbinectedin inhibits the activity of EWS/FLI1, we initially interrogated

the nuclear localization of EWS/FLI1 after treatment. We performed confocal microscopy experiments with lurbinectedin at the same concentration and time that lead to EWS/FLI1 re-localization with trabectedin treatment. Similar to trabectedin, after treatment of Ewing sarcoma cells with 5 nM of lurbinectedin for six hours, EWS/FLI1 accumulates in the nucleolus (Figure 15). Based on the clinical trial report, 5 nM of lurbinectedin should be easily achieved in patients since the maximum tolerated dose was approximately 215 nM (162).

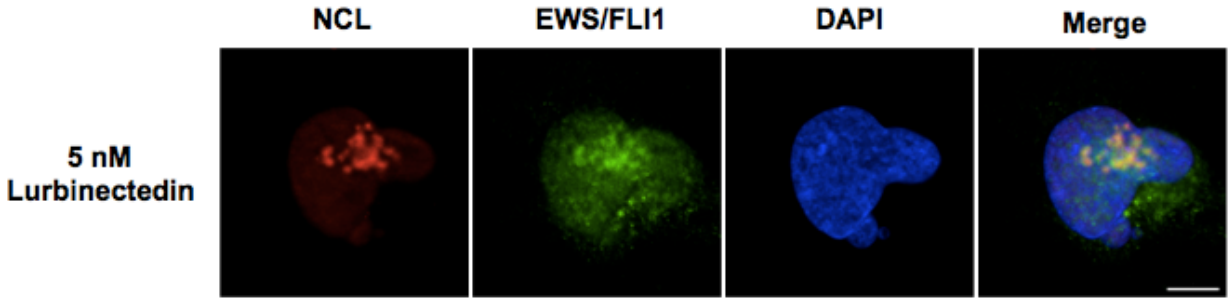

Figure 15: EWS/FLI1 re-localizes after lurbinectedin treatment. Single cell imaging by confocal microscopy displays EWS/FLI1 localization in TC32 cells after 6 hours of treatment with 5 nM lurbinectedin. NCL, Nucleolar marker. DAPI, nuclear marker.

Seeing that trabectedin-mediated re-localization of EWS/FLI1 leads to inhibition, we next examined the functional status of EWS/FLI1 after lurbinectedin-mediated re-localization at the target gene level. To demonstrate the re-localization of EWS/FLI1 induced by lurbinectedin leads to abrogated EWS/FLI1 activity, we treated Ewing sarcoma cells with decreasing concentrations of lurbinectedin for 8 hours and showed specific suppression of luciferase signal driven by an EWS/FLI1-responsive promoter (NR0B1-Luc) (Figure16A, black bars). In parallel, we showed a negligible effect on a constitutively active promoter (CMV-Luc), whose suppression would indicate global transcription inhibition (Figure 16A, gray bars). The observed suppression of EWS/FLI1 activity is dose-dependent and correlates with the concentrations that are required for

re-localization. Additionally, there is no effect of lurbinectedin on overall cell viability at these concentrations and time points as measured by standard MTS assay (Data not shown).

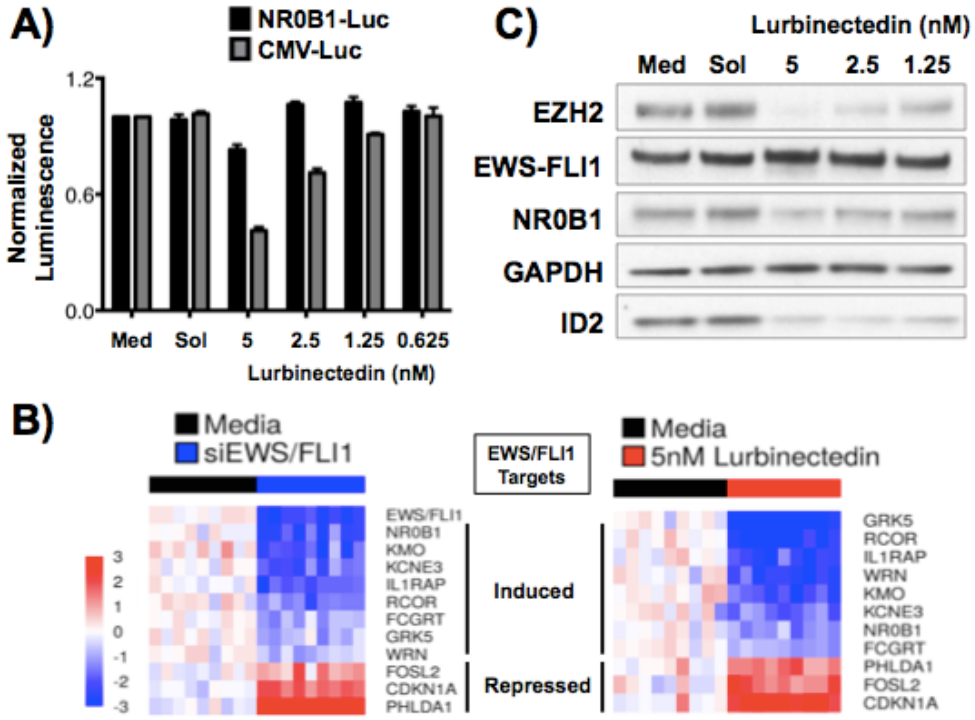

Figure 16: Lurbinectedin inhibits EWS/FLI1 activity at multiple levels. A) In a dose-dependent fashion, 8 hours of lurbinectedin inhibits EWS/FLI1 activity at the NR0B1 promoter, but not the CMV promoter. MTS assays were performed in parallel to ensure the decrease in luciferase signal was not a result of cell death. B) Left, Heatmap of qRT-PCR data demonstrating the effect of EWS/FLI1 knockdown on the expression level of target genes. Right, Heatmap of qRT-PCR data demonstrating the effect of 5nM lurbinectedin for 12 hours on target gene expression. C) Western blot showing the effect of 18 hour lurbinectedin treatment on target protein levels. Cells were treated with the indicated concentration of lurbinectedin.

While the above assay demonstrates the ability of lurbinectedin to block the transactivating activity of EWS/FLI1, EWS/FLI1 also represses expression of numerous target genes. Therefore, in order for a drug to be considered a bonafide EWS/FLI1 inhibitor, it should lead to induction of EWS/FLI1-repressed genes and repression of EWS/FLI1-induced genes. To test the ability of lurbinectedin to completely block activity of EWS/FLI1, we treated Ewing sarcoma cells for 12 hours and measured the change in gene expression of a panel of well-defined EWS/FLI1 targets. Importantly, our gene

signature included genes that are induced by EWS/FLI1 and genes that are repressed by EWS/FLI1. To validate that the genes in the gene signature represent legitimate EWS/FLI1 targets, we eliminated expression of EWS/FLI1 by siRNA and measured the change in expression of each target gene by qRT-PCR (Figure 16B, left). As expected, upon knock down of EWS/FLI1 the induced target genes were repressed and the repressed target genes were induced (Figure 16B, right). We observed the same gene expression changes upon lurbinectedin treatment, supporting our hypothesis that lurbinectedin is an inhibitor of EWS/FLI1 activity. Additionally, the changes in mRNA level correlated with changes at the protein level (Figure 16C).

We confirmed the inhibition of EWS/FLI1 activity across the genome by performing RNA-sequencing. For this experiment, we treated ES cells with lurbinectedin for either 6 or 12 hours and measured the change in expression of nearly 200 EWS/FLI1 target genes. At 6 or 12 hours after treatment with lurbinectedin, we observe a marked repression of EWS/FLI1 induced target genes (80% of target genes are suppressed) (Figure 17).

Intriguingly, the EWS/FLI1 repressed gene signature did not show clear induction of all of the targets. However, target genes repressed by EWS/FLI1 that have been well characterized were induced by lurbinectedin treatment (data not shown). The failure to show induction of the repressed genes could be the result of many factors. The most well-characterized and studied target genes of EWS/FLI1 are induced genes, and there are currently no exhaustive lists of repressed targets. Additionally, the EWS/FLI1-repressed genes identified thus far were detected many days after EWS/FLI1 elimination, and it is unclear if these targets are directly or indirectly linked to EWS/FLI1

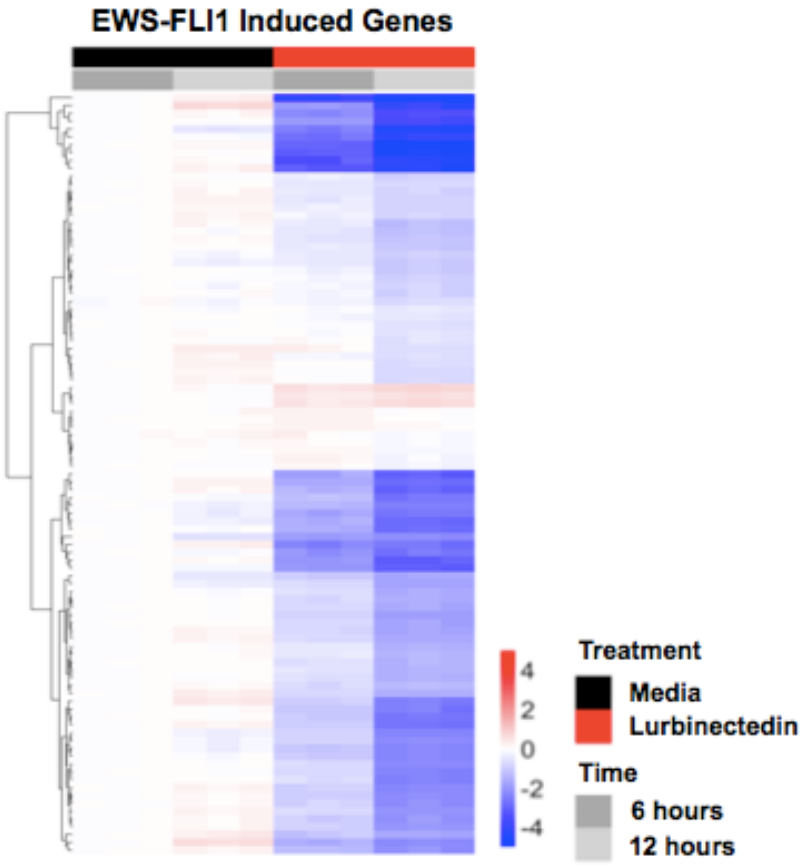

Figure 17: Lurbinectedin suppresses the EWS/FLI1-induced target gene signature. Heatmap representation of RNA-sequencing data shows that the expression of the majority of target genes that are induced by EWS/FLI1 decreases at 6- and 12-hours relative to media control. Genes shown are differentially expressed when normalized to the 6-hour media samples.

expression (164). The induction of gene expression is thought to be a result of EWS/FLI1 oligomerization on GGAA microsatellite DNA sequences leading to the recruitment of transcriptional activators (46). The repression of gene expression by EWS/FLI1 is thought to occur when EWS/FLI1 competes wild-type ETS transcription factors off of chromatin, leading to a down-regulation of gene expression. It is possible that lurbinectedin differentially affects the ability of EWS/FLI1 to oligomerize at GGAA microsatellites more efficiently than it affects the competition with wild-type ETS transcription factors.

In order to show that the transcriptional effects of lurbinectedin treatment are specific to cells expressing EWS/FLI1, we treated a panel of Ewing sarcoma and non-Ewing sarcoma cell lines with lurbinectedin and examined the change in expression of NR0B1 mRNA. We only observed NR0B1 suppression in cell lines containing EWS/FLI1 (Figure 18). In all other cell lines tested, NR0B1 expression is unchanged or induced by lurbinectedin treatment.

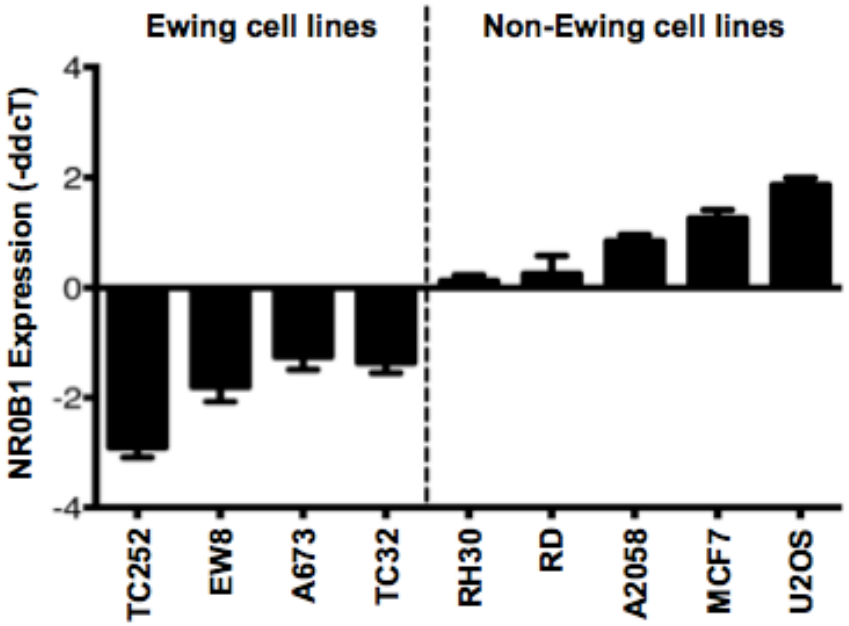

Figure 18: Suppression of NR0B1 expression is specific to Ewing sarcoma cells. Suppression of NR0B1 mRNA after treatment with 5 nM lurbinectedin for 12-hours is restricted to Ewing sarcoma cells. RH30, alveolar rhabdomyosarcoma. RD, embryonal rhabdomyosarcoma. A2058, metastatic melanoma. MCF7, breast cancer. U2OS, osteosarcoma.

We next investigated the ability of lurbinectedin to synergize *in vitro* with SN38, the active metabolite of irinotecan. The mechanism of synergy between trabectedin and irinotecan is dependent upon the suppression of WRN by trabectedin. Therefore, we showed that treatment of Ewing sarcoma cells with lurbinectedin led to a dose-dependent suppression of WRN mRNA expression by qRT-PCR. Similar to trabectedin,

this suppression occurred at the identical concentration that caused re-localization of EWS/FLI1 and loss of activity (Figure 19A).

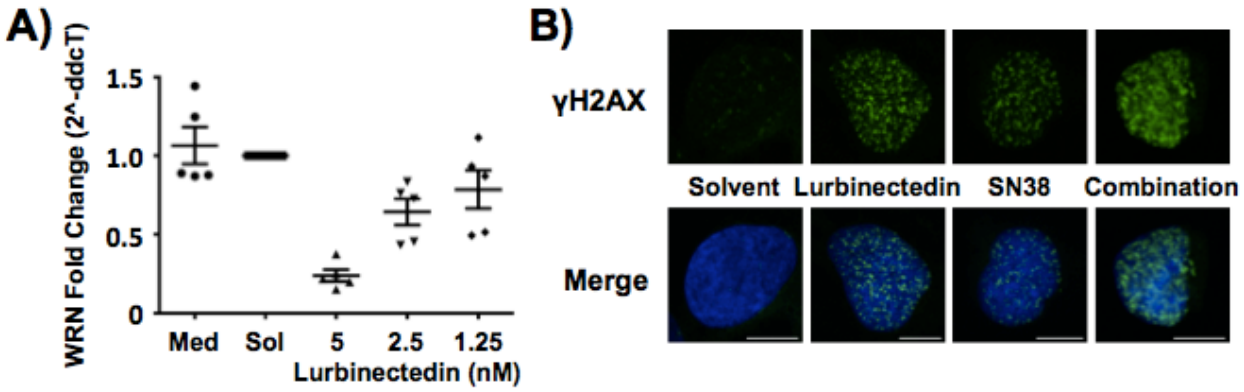

Figure 19: Lurbinectedin suppresses WRN expression and hyper-sensitizes Ewing sarcoma cells to SN38 treatment. A) TC32 cells were treated with the indicated concentration of lurbinectedin for 12-hours. Med, Media. Sol, Solvent. B) Single cell imaging by confocal microscopy demonstrates the generation of γH2A.X upon either 12 hour, 5 nM lurbinectedin or 5 nM SN38 or the combination of the two drugs.

Due to the fact that WRN expression is suppressed following lurbinectedin treatment, Ewing sarcoma cells should be hypersensitive to DNA damage induction using SN38. In order to show this hypersensitivity, we treated Ewing sarcoma cells with 5 nM lurbinectedin, 5 nM SN38, or the combination therapy for 12 hours and measured the generation of γH2A.X foci by confocal microscopy. We showed that Ewing sarcoma cells treated with the combination of lurbinectedin and SN38 display a dramatic increase in γH2A.X foci (Figure 19B).

By definition, synergy can only occur when two compounds affect activity in independent pathways. If the two compounds inhibit the same pathway, then their effects would be considered additive. However, our laboratory and other groups have previously demonstrated that SN38 treatment alone can inhibit EWS/FLI1 activity (114, 165). Therefore, to demonstrate synergy between SN38 and lurbinectedin, we examined the localization of EWS/FLI1 after treatment with SN38. We showed the

minimal inhibition of EWS/FLI1 following treatment with SN38 is not due to EWS/FLI1 re-localization (Figure 20A). Because SN38 does not cause re-distribution of EWS/FLI1 in the nucleus, we believe that two independent mechanisms of action exist. Supporting this hypothesis, we demonstrate ES cells treated with sub-optimal concentrations of both drugs leads to a dramatic decrease of EWS/FLI1 target protein expression (Figure 20B).

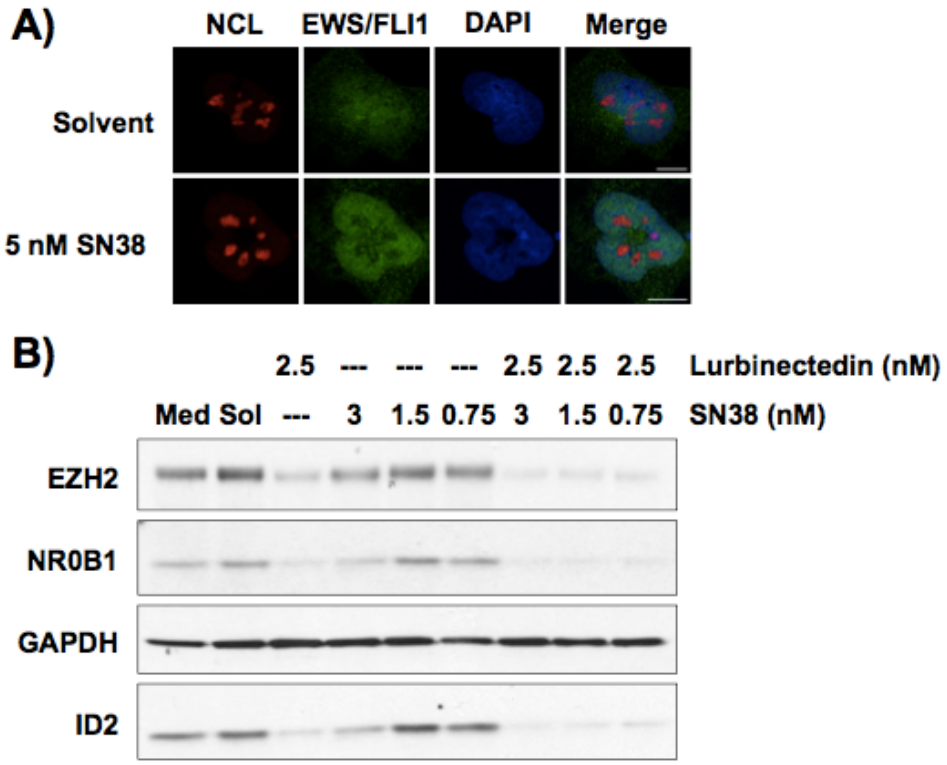

Figure 20: Lurbinectedin and SN38 synergize to suppress EWS/FLI1 activity. A) Single cell imaging of TC32 cells following 5 nM SN38 treatment. Red = NCL, nucleolar marker. Blue = DAPI, nuclear marker. B) TC32 cells were treated with the indicated concentrations of lurbinectedin, SN38, or the combination. EWS/FLI1 target protein expression is shown following 18-hours of treatment.

As a result of the marked activity *in vitro*, we evaluated the combination therapy of lurbinectedin and irinotecan *in vivo* using two Ewing sarcoma xenograft models, TC71 and TC32. Mice were treated with 0.18 mg/kg of lurbinectedin intravenously on days 0 and 7 (TC32) or 0, 7, and 14 (TC71). The TC71 cohort was treated with

irinotecan on days 1-3, 8-10, and 15-17, while the TC32 cohort received irinotecan on days 3 and 10. Irinotecan was administered by intraperitoneal injection at a dose of 5 mg/kg, which is well below the maximum tolerated dose. Using this schedule, we observed delayed tumor growth for both single agent therapies and sustained tumor regression in the combination setting for both xenografts (Figure 21A). We observed minimal toxicity and weight loss with any treatment regimen (data not shown).

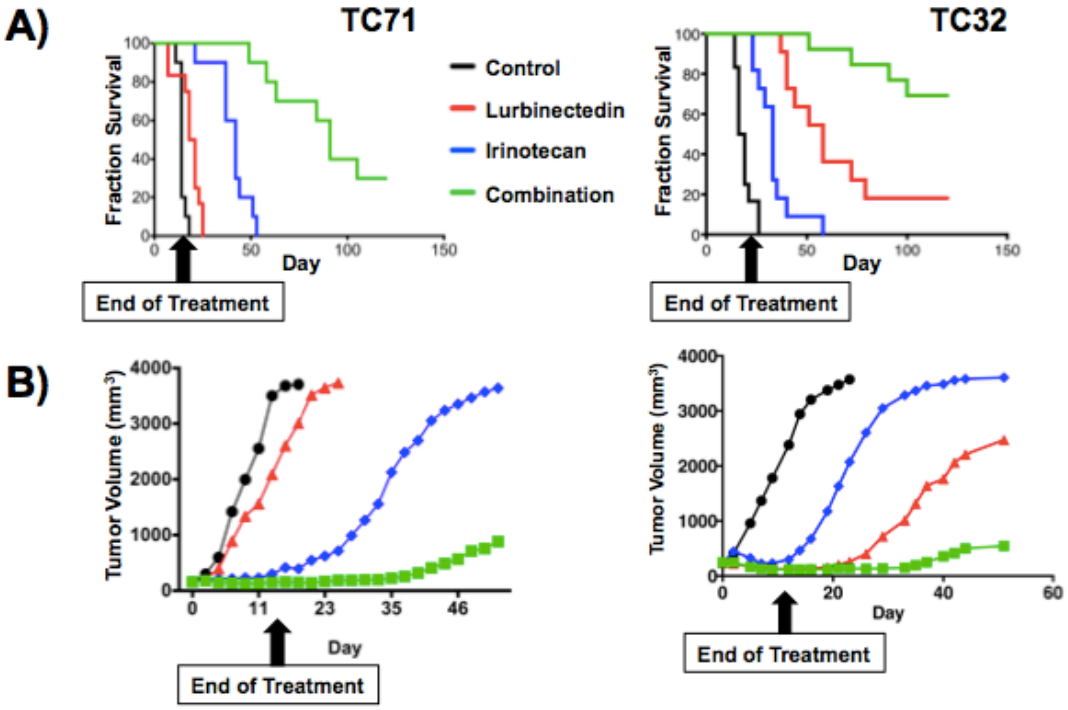

Figure 21: Combination therapy leads to xenograft growth suppression and increased survival *in vivo*. A) Survival curves for mice bearing TC71 (left) or TC32 (right) xenografts. Both cohorts were treated with lurbinectedin on days 0 and 7. TC32 mice were treated with irinotecan on days 3 and 10, whereas TC71mice received an additional dose of lurbinectedin on day 14 and irinotecan on days 1 to 3, 8 to 10, and 15 to 17. All groups survived significantly longer than control (all $P < 0.0001$). P value was determined using Cox proportional hazards regression. B) Average tumor growth curves curves for mice bearing TC71 (left) or TC32 (right) xenografts.

Importantly, decreased tumor burden in the combination setting lead to an increase in overall survival in both xenografts, including complete cures of 30% of the TC71 mice and 70% of the TC32 mice for more than 100 days after the end of therapy (Figure 21B).

To demonstrate the on-target effect of EWS/FLI1 inhibition with lurbinectedin treatment *in vivo*, we developed an immunofluorescent assay that quantitatively measures the expression of NR0B1 protein in xenograft tumors during treatment. To validate this assay, we treated Ewing sarcoma cells *in vitro* with a siRNA to NR0B1. We showed decreased NR0B1 signal in the single agent lurbinectedin cohort relative to the mice treated with vehicle on day 3 (Figure 22). This proves that lurbinectedin acts as an EWS/FLI1 inhibitor *in vitro* as well as *in vivo*.

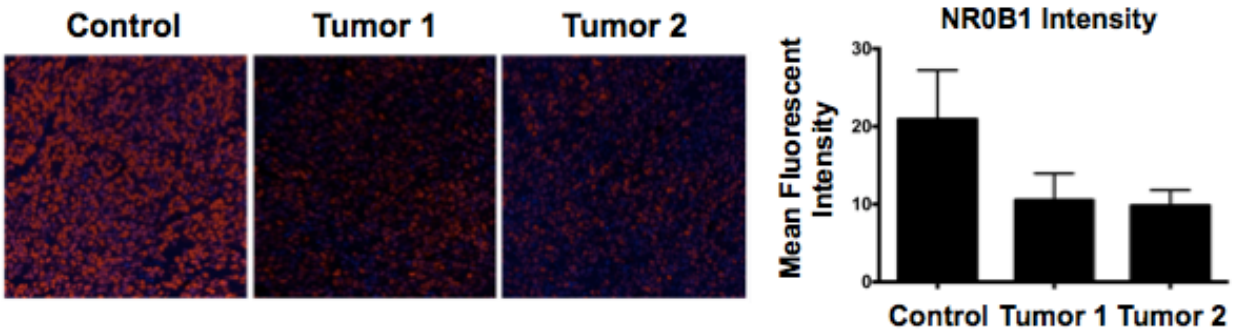

Figure 22: Lurbinectedin inhibits EWS/FLI1 activity *in vivo*. Representative immunofluorescence images of lurbinectedin-treated tumors stained for NR0B1 expression 3 days after initial treatment. Intensity of immunofluorescence is quantified on the right.

In order to explain the durable effect of the combination therapy, we analyzed the morphology of the tumors over time. Surprisingly, we identified a time-dependent replacement of tumor tissue with benign adipocytes (Figures 23A). We identified zones of active differentiation, and showed these areas stain positive for two different markers of human origin, ALU-ish (human DNA marker) and a human-specific mitochondrial protein marker (Figure 23B). This is consistent with a complete block in EWS/FLI1 activity that has been previously shown to result in differentiation of Ewing sarcoma cells (8, 61).

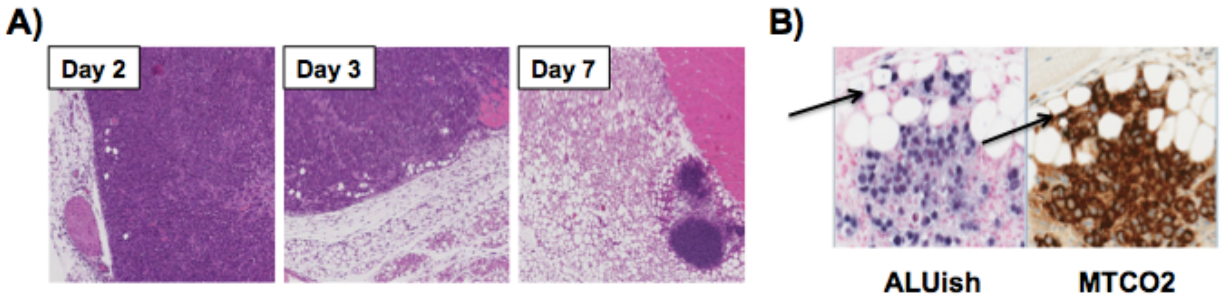

Figure 23: Combination therapy induces adipogenic differentiation. A) Hematoxylin and eosin staining demonstrates differentiation of TC71 Ewing sarcoma xenograft over time into adipose tissue in mice treated with the combination therapy. B) Xenograft sections were stained with 2 separate markers of human origin to prove the presence of human fat in mice. Left, ALUish DNA probes for human-specific ALU repeat sequences. Right, MTCO2, Human mitochondrial surface stain. Images acquired at 20X.

While the vast majority of adipocytes were mouse in origin, it appeared that the mouse fat gradually replaced the human fat in these xenografts. This is in agreement with known remodeling that occurs when human mammary xenografts are transferred into immunocompromised mice (166). Additionally, we identified these areas stain positive for Ki67, a proliferative marker, and do not stain for cleaved caspase 3, a marker of cell death (data not shown). This data argues that the combination therapy leads to a complete block in EWS/FLI1 activity, which suppresses the proliferation of the tumor and induces their ability to differentiation down the mesenchymal lineage. While the ability of Ewing sarcoma cells to differentiate *in vitro* has been observed by many laboratories, to our knowledge, this is the first time that a molecularly targeted combination therapy has been reported to effectively cure a proportion of well-established Ewing sarcoma xenografts by differentiating the tumor into a mesenchymal tissue type (8, 61). This is clinically relevant because the introduction of differentiation therapies into the clinic in other tumor types, most notably acute promyelocytic leukemia, has seen the long-term overall survivor rate increase to over 90% (127).

Finally, we needed to ensure the differentiation phenotype observed *in vivo* was a result of the cell's ability to differentiate in response to drug treatment. To this end, we developed an *in vitro* model of adipogenic differentiation that utilized transient (1-hour) treatment with 10 nM lurbinectedin followed by incubation with regular cell culture medium to re-capitulate the exposure to drug that the mice experienced. The lurbinectedin washout model lead to delayed cell growth as measured by percent confluence and distinct changes in cell morphology. In particular, a subset of cells appeared to accumulate large, round lipid droplets that are indicative of adipocytes (Figure 24A).

In addition to the phenotypic changes, we examined the mRNA expression level of the well-characterized master regulator of terminal differentiation for adipose tissue, PPARG (167). We showed transient treatment of Ewing sarcoma cells with lurbinectedin followed by normal medium lead to a marked induction of PPARG (Figure 24B). To prove that the up-regulation of PPARG and altered morphology were activating an adipogenic program, we stained the Ewing sarcoma cells with two distinct neutral lipid markers, BODIPY and Oil Red O. We were able to show two days after lurbinectedin washout treatment, nearly 100% of the cells remaining were producing and accumulating lipid (Figures 24C and D).

These results re-capitulated what we observed *in vivo* and corroborated what other laboratories have demonstrated with EWS/FLI1 knockdown. Importantly, the *in*

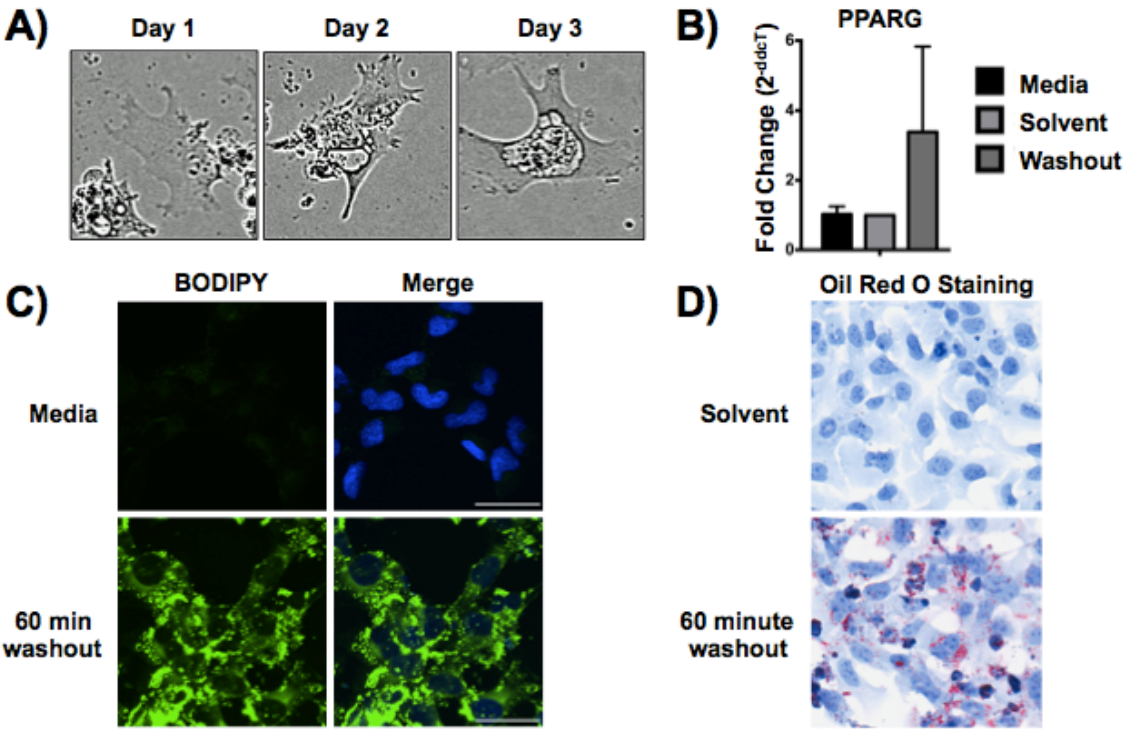

Figure 24: Transient lurbinectedin treatment induces adipogenesis *in* vitro. A) Images of TC32 cells treated with 10 nM lurbinectedin for 1-hour and followed by incubation with regular cell culture medium. Images were acquired at the indicated day after drug washout. B) Treatment of TC32 cells with 10 nM lurbinectedin for 1-hour leads to increased expression of PPARG mRNA. C) Confocal imaging of BODIPY dye 48-hours after lurbinectedin was removed from the media. BODIPY, neutral lipid stain. Hoescht, DNA marker. D) Oil Red O images compare solvent to lurbinectedin washout 48-hours after drug removal. Images were acquired at 20X magnification.

vitro exposures after lurbinectedin washout are reflective of the exposures observed in the xenograft experiments, although higher concentrations and longer exposures should be feasible in patients because of the improved pharmacokinetic profile of lurbinectedin. These data prove that lurbinectedin is a bona fide EWS/FLI1 inhibitor that should be pursued for clinical testing in Ewing sarcoma patients.

Conclusions

We have identified a second-generation structural analog of trabectedin, lurbinectedin, that has an improved pharmacokinetic profile. Lurbinectedin can be administered to patients at a higher dose during a 1-hour infusion schedule before

reaching the dose limiting toxicities that hamper the drug's efficacy. The schedule of administration and decreased toxicity profile significantly increase the concentration of drug that a patient can tolerate to nearly 20-times the maximum concentration of trabectedin.

Prior to our studies, the ability of lurbinectedin to function as an EWS/FLI1 inhibitor had not been addressed. We demonstrated that lurbinectedin treatment does inhibit EWS/FLI1 activity, and this inhibition is a result of the same EWS/FLI1 re-localization mechanism that we previously characterized with trabectedin treatment. The fact that re-localization occurs at identical concentrations *in vitro* is promising, because lurbinectedin is far less toxic in patients and can achieve much higher serum concentrations.

We demonstrated that lurbinectedin-induced EWS/FLI1 re-localization correlated with target gene and protein suppression. Additionally, we showed that lurbinectedin treatment suppressed the expression of the WRN helicase, which sensitized Ewing sarcoma cells to treatment with SN38 (*in vitro*) or irinotecan (*in vivo*). The combination of the two drugs targeted DNA damage to ES cells and suppressed EWS/FLI1 activity by at least two independent mechanisms. When the combination is evaluated in Ewing sarcoma xenografts, we observed greatly improved survival and tumors that were gradually replaced by adipose tissue. We showed that a portion of the adipose tissue was human in origin, and re-capitulated the process of lurbinectedin-induced adipogenesis *in vitro*.

The most important result from these studies is the observation that a block in EWS/FLI1 activity leads to the differentiation of tumor cells into adipose tissue. The

newly created adipose tissue contains the same DNA as Ewing sarcoma cells, and thus should continue to express the EWS/FLI1 protein; however, as we demonstrated, EWS/FLI1 protein is functionally inactivated following treatment. It is possible that the re-localization of EWS/FLI1 creates a window of time during which epigenetic changes can occur that permanently reshape the chromatin leading to sustained effects on gene expression. In support of this, we know that EWS/FLI1 activity affects the expression of important epigenetic readers and writers, and the nucleolar enrichment of EWS/FLI1 is transient following lurbinectedin treatment (Data not shown). Additionally, it is well known that the epigenetic landscape is significantly altered as early mesenchymal progenitor cells terminally differentiate (168-172).

Considering the combination of lurbinectedin and irinotecan leads to the differentiation of adipose tissue, it will be important to re-consider the parameters used to detect drug activity in early phase clinical testing. Currently, the net change in solid tumor volume is the most widely utilized readout to measure the activity of a drug (173). While this system works well for most chemotherapy that is cytotoxic and lead to an overall reduction in tumor burden, a different endpoint needs to be developed for differentiation therapies that may not bring about reduced tumor volumes. Our laboratory has recently developed an imaging-based biomarker readout to detect changes in the activity of EWS/FLI1 (174).

While we have characterized the mechanism of EWS/FLI1 inhibition in response to lurbinectedin treatment, it will be important in the future to more completely characterize the contribution of irinotecan to this synergistic combination therapy. Irinotecan has been well studied and clinically developed because of its capacity to

inhibit DNA topoisomerase I by generating cleavage complexes that result in DNA damage. It is unlikely that topoisomerase I inhibition is a dominant mechanism in this combination setting because of the low concentration of SN38 or irinotecan used in these studies. In fact, *in vitro* experiments that aim to inhibit topoisomerase I generally use much higher concentrations (micromolar) to create topoisomerase I cleavage complexes (175).

CHAPTER 5

Materials and Methods

Cell Lines and Culture Reagents

All Ewing sarcoma cell lines except TC252, TC253, and A4573 were obtained from Dr. Lee J. Helman (National Cancer Institute, Bethesda, MD). Dr Helman also gifted the RH30 and RD cell lines. All other Ewing sarcoma cell lines were the gift of Dr. Tim Triche (The Saban Research Hospital, Children's Hospital of Los Angeles). MCF7 cells were the gift of Dr. P. Steeg (National Cancer Institute, Bethesda, MD). A2058 were purchased from ATCC. All cell lines were routinely screened to confirm mycoplasma negative status and to confirm the identity of the cells by STR profiling (DDC Medical). STR testing was performed on 11/30/14 for all the cells except A2058, which was tested 2/12/16. EWS/FLI1 expression was confirmed by RT-PCR. Cells were grown at 37 °C with 5% CO_2. RPMI-1640 (Gibco) was supplemented with 10% fetal bovine serum (Gemini Bio-Products), 2 mM L-glutamine, and 100 U/mL and 100 µg/mL penicillin and streptomycin, respectively (Gibco). siRNA experiments were conducted in media without antibiotics.

Small, Interfering RNA (siRNA) Treatment

A custom-designed siRNA targeting the breakpoint of EWS/FLI1, Allstars Negative Control siRNA, and Allstars Hs Cell Death Control siRNA were purchased from Qiagen (Hilden, Germany). All siRNAs were purchased lyophilized and diluted with sterile water to a concentration of 20 µM. The final, working concentration of siRNA in each experiment was 20 nM. For experiments, individual siRNAs were incubated with Lipofectamine RNAiMAX Transfection Reagent from Invitrogen (Carlsbad, CA, USA) for

30 minutes. After 30 minutes, Ewing sarcoma cells were added to the siRNA/Lipofectamine mixture at a pre-determined density. Cells were allowed to grow in the presence of the siRNA for 24 hours before RNA was collected.

Compounds

Trabectedin, Lurbinectedin, and ET-745 were gifted from Pharmamar (Madrid, Spain). Lyophilized compound was dissolved in DMSO to a stock of 1 mg/mL, and working solutions were made up to 10 μM. Etoposide was purchased from Sigma-Aldrich (St. Louis, MO, USA) and dissolved to a working solution of 1 mM in DMSO. SN38 was purchased from Sigma-Aldrich (St. Louis, MO, USA) and dissolved to a working solution of 50 μM in DMSO. For all experiments, stock solutions obtained from the -20^{o}C freezer were thawed and diluted in cell culture medium prior to use.

Confocal microscopy

TC32 cells were incubated with drug for 1 hour followed by incubation with regular media or 6 hours continuously in a Nunc Lab-Tek II Chamber Slide (Thermo Scientific), fixed in 4% paraformaldehyde in PBS, washed, lysed in 0.1% Triton-X100, and blocked in 10% goat serum (all in PBS). The cells were incubated with primary antibody (18 hours), secondary antibody (1 hour) and tertiary antibody for 30 min with washes in between followed by mounting in ProLong Gold with DAPI (Life Technologies);(Primary antibodies: nucleolin, Abcam – 1:1000; HA-tag, Abcam – 1:500; γH2AX, Millipore – 1:1000; FLI1, Abcam – 1:100; H3K9me3, Abcam – 1:2000)(Secondary antibodies: biotin anti-mouse IgG: Vector – 1:1000)(Tertiary antibodies: Strep-635, Life Technologies – 1:400; FITC-Rabbit, Millipore – 1:200). All images were obtained with standardized settings on a Zeiss 510 confocal microscope. For BODIPY images, TC32 cells were treated as indicated. 1 hour prior to fixation in 4%

paraformaldehyde, BODIPY 493/503 (Invitrogen) and Hoechst 33342 (Invitrogen) were added to the culture medium. The cells were washed, cover slips were placed on the slides, and the slides were subsequently imaged.

Cell Proliferation Assays

Cell viability IC50s were determined by non-linear regression (Prism GraphPad) as the average of three independent experiments using standard MTS assay CellTiter 96 (Promega) following a 48 hour incubation with drug as previously described. (85) Real time proliferation assays were performed on the Incucyte Zoom™ as previously described. (86)

Luciferase Assays

Ewing sarcoma cell lines stably expressing an EWS/FLI1-driven NR0B1 luciferase or constitutively active CMV-driven control were incubated with drug in opaque 96 well plates (BD Falcon) for 8 hours. (85) Cells were lysed in 100 µL of Steady-Glo (Promega) and bioluminescence was measured on a BioTek plate reader (Winooski, VT).

Quantitative RT-PCR

300,000 cells were incubated with drug in 6-well plates (BD Falcon, Franklin Lakes, NJ). RNA was collected using the RNeasy kit (Qiagen), and immediately reverse-transcribed using a high-capacity reverse transcriptase kit (Life Technologies) at 25 °C for 10 min, 37 °C for 120 min, and 85 °C for 10 min. We subsequently PCR amplified 100 ng of cDNA, 2X SYBR green (Bio-Rad), and the following program: 95 °C for 10 min, 95 °C for 15 s, 55 °C for 15 s, and 72 °C for 1 min, for 40 cycles. Expression was determined from three independent experiments relative to GAPDH and solvent

control using standard ddCt methods. Primers sequences can be found in the table below:

Gene Name	Forward Primer	Reverse Primer
EWS/FLI1	CGACTAGTTATGATCAGAGCAGT	CCGTTGCTCTGTATTCTTACTGA
NR0B1	CAGTGGGGAACTCAGCAAAT	ATCATCCATGCTGACTGTGC
KMO	TGCTGAGAAATACCCCAATGTG	CTGACAGTTGAATAGGCTCCATC
KCNE3	AGACTACCAATGGAACGGAGA	GCGGGTGTATCCCAGGATG
IL1RAP	ATTCTCGCAATGAGGTTTGG	CAGACATAGCTGCGCTTGAG
RCOR	GGTGGCTTTGAACACTTGGT	GTGGAGCTCTCTGGGAAGTG
FCGRT	GATGAGCACCACTACTGCTG	CAAGACACCGATGACGATTCC
GRK5	CCCAAAGTCCCCTGTTTTCAT	ATTCGTGGAATGGTTCTCCCC
WRN	TCGCAGGCACAGTTTATTTG	GGCAGAAGCAACTTCTTTGG
FOSL2	CAGAAATTCCGGGTAGATATGCC	GGTATGGGTTGGACATGGAGG
CDKN1A	TGTCCGTCAGAACCCATGC	AAAGTCGAAGTTCCATCGCTC
PHLDA1	GGAGATCGACTTTCGGTGCC	GGCCTGACGATTCTTGTACTG
BCL11B	GGTGCCTGCTATGACAAGG	GGCTCGGACACTTTCCTGAG
LOX	CGGCGGAGGAAAACTGTCT	TCGGCTGGGTAAGAAATCTGA
PRKCB	AAACCTTGTACCTATGGACCCC	CCCAATCCCAAATCTCTACTGAC
STEAP2	CAAGCGCGACAACAGGTTATT	CAGAGAGTAAAGAGTCGTAGGGG

All PCR products were validated by gel electrophoresis followed by standard Sanger sequencing. Data illustrated in heat map format were created using R v 3.2.2 (R Foundation for Statistical Computing, Vienna, Austria) and comprise delta-delta Ct scores truncated between -3 and 3 to prevent very large scores from oversaturating the color gradient.

Western Blotting

1.5 million cells were incubated with the indicated concentration of drug in 10 cm^2 dishes, scraped into cold PBS, washed in PBS and lysed in 4% LDS lysis buffer. Following dilution of detergent, the protein was quantitated using the bicinchoninic (BCA) colorimetric assay (Pierce, Thermo-Scientific). 30 µg of total protein were resolved on a NuPage 4% to 12% Bis-Tris gradient gel (Invitrogen) in 1X NuPage MOPS SDS Running Buffer (Invitrogen), transferred to nitrocellulose using 1X Tris-

Glycine-SDS Buffer (Bio-Rad) supplemented with 20% methanol at 4 °C overnight at 20 V. The membranes were subsequently blocked in 5% milk in TBS-T, and probed with Abcam (FLI1, NR0B1, and GAPDH) or Cell Signaling (EZH2 and ID2) antibodies.

Alternatively, for nuclear extraction western blots cells were plated, treated, scraped and washed as stated above. TC32 cells were incubated in 500 µl of cytoplasmic lysis buffer (10 mM HEPES, pH=7.9, 50 mM KCl, 0.1 mM EDTA, 0.1% NP-40 in PBS) for 5 minutes. After spinning at 1000 G for 5 minutes at 4^{o}C, soluble nuclear extraction buffer (50 mM HEPES, pH=7.5, 150mM NaCl, 1mM EDTA, 0.5% NP-40) was added according to the size of the pellet and allowed to sit on ice for 30 minutes. Extracts were centrifuged at 4^{o}C for 10 minutes at 15000 G. Following centrifugation, samples were boiled in 4% LDS sample buffer for 10 minutes to extract the insoluble nuclear fraction. 10 µg of insoluble nuclear protein were resolved and block as stated above. Abcam antibodies (SUV39H2, HP1α, and H3K9me3) were used for detection.

Xenograft Experiments

Two million cells were injected intramuscularly in the gastrocnemius of female 4-6-week old female homozygous nude mice (Crl; Nu-*Foxn1*^{Nu})(Harlan Laboratories, SL) and established to a minimum diameter of 0.5 cm. Four cohorts of 12 mice were treated with vehicle, lurbinectedin (0.18 mg/kg intravenously; TC32 days 0, 7; TC71 days 0, 7, 14), irinotecan (5 mg/kg intraperitoneal; TC32 days 3, 10; TC71 days; 1 to 3, 8 to 10; 15 to 17) or the combination (same dose route and schedule as the individual tumor types). Tumor volume was measured 3 times per week and determined using the equation (D x d^2)/6 × 3.12 (where D is the maximum diameter and d is the minimum diameter). Tissue was collected and fixed in 10% formalin. Mice were sacrificed when the tumor diameter reached 2 cm in any dimension. All experiments were performed in

accordance with the guidelines and regulation of, and approved by the animal care and use committee (PharmaMar). Investigators were not blinded to the treatment groups.

Tissue Staining

Paraffin embedded tissue was sectioned into 5-micrometer sections and mounted on colormark plus charged slides. Antigen retrieval was performed in Ventana CC1 or manually for IF using citrate buffer (Dako). Following blocking, the tissue was incubated with NR0B1 primary (Abcam, 1:50) washed and then secondary antibody (Anti-Rabbit Cy5 conjugated, Life Technologies).

Oil Red O Staining

TC32 cells were plated and treated in Nunc Lab-Tek II Chamber Slides (Thermo Scientific). Cells were washed with PBS, fixed for 30 minutes, and then washed with distilled water. Cells were incubated with isopropanol for 3 minutes and a working solution (filtered 3:2 Oil Red O (Sigma) to deionized water) of Oil Red O for 10 minutes. After aspirating the oil red o solution, the slides were briefly stained with hematoxylin solution (Sigma) and imaged using an Aperio scanning microscope (Leica, Buffalo Grove, IL).

Immunofluorescence and Immunohistochemistry

Paraffin embedded tissue was sectioned into 5-micrometer sections and mounted on colormark plus charged slides. Antigen retrieval was performed on Ventana Discovery Automated Stainer. Immunofluorescence staining was performed using NR0B1 primary (Abcam, 1:300), Ventana Ultramap Rb HRP and Ventana Discovery Cy5 amplification. Immunohistochemistry was performed using Ki67 (Spring Bioscience, 1:100) and Cleaved Caspase-3 (Cell Signaling, 1:400) primary antibodies, VentanaUmap rb HRP and VentanaChromomap DAB.

Immunofluorescence Quantitation

Fluorescent images were acquired at 20x magnification using the PE Vectra automated multispectral slide imager. Fluorescence was quantitated using Inform software. Standard settings were used for across all treatments for image acquisition and quantitation.

RNA-Sequencing

RNA was extracted from three biological replicates for each experimental time point and samples were submitted for 1X 75 bp sequencing on the Illumina NextSeq 500 at the Van Andel Research Institute. Sequencing libraries were prepared using the Illumina TruSeq HT kit. Read quality was assessed using FASTQC v. 0.11.3 and aligned to the hg19 genome using Subread v. 1.4.3. with default parameters (176). Raw read counts to known exons were obtained using FeatureCounts v 1.4.3 using strand specific read counting. Counts per million (CPM) were calculated and log2 transformed using voom (177). Transformation and differential expression analyses were conducted using the limma package v 3.28.7 in R (178). The EWS/FLI1 gene signature consists of all genes in common from two data sets: a meta-analysis and a list of differentially expressed genes obtained by expression profiling following silencing of EWS/FLI1 in 5 cell lines (51, 164). 116 and 50 genes were identified as induced or repressed by EWS/FLI1, respectively. Significance testing for enrichment of EWS/FLI1 induced or repressed gene signatures from differentially expressed genes were performed using a hypergeometric test with the phyper function implemented in the R stats package (v 3.3.0) (https://cran.r-project.org/). Heatmaps were generated using either the aheatmap function implemented in the NMF package (v 0.20.6) or the pheatmap package (v 1.0.8) in R (v 3.3.0).

REFERENCES

1. Riggi N, Stamenkovic I. The Biology of Ewing sarcoma. Cancer Lett. 2007;254(1):1-10.

2. Zamora P, Garcia de Paredes ML, Gonzalez Baron M, Diaz MA, Escobar Y, Ordonez A, et al. Ewing's tumor in brothers. An unusual observation. Am J Clin Oncol. 1986;9(4):358-60.

3. Ewing J. Classics in oncology. Diffuse endothelioma of bone. James Ewing. Proceedings of the New York Pathological Society, 1921. CA Cancer J Clin. 1972;22(2):95-8.

4. Coley BL, Higinbotham NL, Bowden L. Endothelioma of bone; Ewing's sarcoma. Ann Surg. 1948;128(3):533-60.

5. Esser SM, Baima J. Ewing sarcoma causing back and leg pain in 2 patients. PM R. 2012;4(4):317-21.

6. Desai SS, Jambhekar NA. Pathology of Ewing's sarcoma/PNET: Current opinion and emerging concepts. Indian J Orthop. 2010;44(4):363-8.

7. Triche TJ, Askin FB. Neuroblastoma and the differential diagnosis of small-, round-, blue-cell tumors. Hum Pathol. 1983;14(7):569-95.

8. Tirode F, Laud-Duval K, Prieur A, Delorme B, Charbord P, Delattre O. Mesenchymal stem cell features of Ewing tumors. Cancer Cell. 2007;11(5):421-9.

9. Pinto A, Dickman P, Parham D. Pathobiologic markers of the ewing sarcoma family of tumors: state of the art and prediction of behaviour. Sarcoma. 2011;2011:856190.

10. Le Douarin NM, Calloni GW, Dupin E. The stem cells of the neural crest. Cell Cycle. 2008;7(8):1013-9.

11. von Levetzow C, Jiang X, Gwye Y, von Levetzow G, Hung L, Cooper A, et al. Modeling initiation of Ewing sarcoma in human neural crest cells. PLoS One. 2011;6(4):e19305.

12. Bernstein M, Kovar H, Paulussen M, Randall RL, Schuck A, Teot LA, et al. Ewing's sarcoma family of tumors: current management. Oncologist. 2006;11(5):503-19.

13. DuBois SG, Krailo MD, Lessnick SL, Smith R, Chen Z, Marina N, et al. Phase II study of intermediate-dose cytarabine in patients with relapsed or refractory Ewing

sarcoma: a report from the Children's Oncology Group. Pediatr Blood Cancer. 2009;52(3):324-7.

14. Wexler LH, DeLaney TF, Tsokos M, Avila N, Steinberg SM, Weaver-McClure L, et al. Ifosfamide and etoposide plus vincristine, doxorubicin, and cyclophosphamide for newly diagnosed Ewing's sarcoma family of tumors. Cancer. 1996;78(4):901-11.

15. Gaspar N, Hawkins DS, Dirksen U, Lewis IJ, Ferrari S, Le Deley MC, et al. Ewing Sarcoma: Current Management and Future Approaches Through Collaboration. J Clin Oncol. 2015;33(27):3036-46.

16. Ahmed SK, Robinson SI, Okuno SH, Rose PS, Laack NN. Adult ewing sarcoma: survival and local control outcomes in 102 patients with localized disease. Sarcoma. 2013;2013:681425.

17. Lawson M, Vasilaras A, De Vries A, Mactaggart P, Nicol D. Urological implications of cyclophosphamide and ifosfamide. Scand J Urol Nephrol. 2008;42(4):309-17.

18. Lotrionte M, Biondi-Zoccai G, Abbate A, Lanzetta G, D'Ascenzo F, Malavasi V, et al. Review and meta-analysis of incidence and clinical predictors of anthracycline cardiotoxicity. Am J Cardiol. 2013;112(12):1980-4.

19. Crompton BD, Stewart C, Taylor-Weiner A, Alexe G, Kurek KC, Calicchio ML, et al. The genomic landscape of pediatric Ewing sarcoma. Cancer Discov. 2014;4(11):1326-41.

20. Brohl AS, Solomon DA, Chang W, Wang J, Song Y, Sindiri S, et al. The genomic landscape of the Ewing Sarcoma family of tumors reveals recurrent STAG2 mutation. PLoS Genet. 2014;10(7):e1004475.

21. Tirode F, Surdez D, Ma X, Parker M, Le Deley MC, Bahrami A, et al. Genomic landscape of Ewing sarcoma defines an aggressive subtype with co-association of STAG2 and TP53 mutations. Cancer Discov. 2014;4(11):1342-53.

22. Lawrence MS, Stojanov P, Polak P, Kryukov GV, Cibulskis K, Sivachenko A, et al. Mutational heterogeneity in cancer and the search for new cancer-associated genes. Nature. 2013;499(7457):214-8.

23. Mackintosh C, Ordonez JL, Garcia-Dominguez DJ, Sevillano V, Llombart-Bosch A, Szuhai K, et al. 1q gain and CDT2 overexpression underlie an aggressive and highly proliferative form of Ewing sarcoma. Oncogene. 2012;31(10):1287-98.

24. Muller PA, Vousden KH. p53 mutations in cancer. Nat Cell Biol. 2013;15(1):2-8.

25. Solomon DA, Kim T, Diaz-Martinez LA, Fair J, Elkahloun AG, Harris BT, et al. Mutational inactivation of STAG2 causes aneuploidy in human cancer. Science. 2011;333(6045):1039-43.

26. Delattre O, Zucman J, Plougastel B, Desmaze C, Melot T, Peter M, et al. Gene fusion with an ETS DNA-binding domain caused by chromosome translocation in human tumours. Nature. 1992;359(6391):162-5.

27. Abedin MJ, Nguyen A, Jiang N, Perry CE, Shelton JM, Watson DK, et al. Fli1 acts downstream of Etv2 to govern cell survival and vascular homeostasis via positive autoregulation. Circ Res. 2014;114(11):1690-9.

28. Rao AK. Spotlight on FLI1, RUNX1, and platelet dysfunction. Blood. 2013;122(25):4004-6.

29. Hoell JI, Larsson E, Runge S, Nusbaum JD, Duggimpudi S, Farazi TA, et al. RNA targets of wild-type and mutant FET family proteins. Nat Struct Mol Biol. 2011;18(12):1428-31.

30. Lin PP, Brody RI, Hamelin AC, Bradner JE, Healey JH, Ladanyi M. Differential transactivation by alternative EWS-FLI1 fusion proteins correlates with clinical heterogeneity in Ewing's sarcoma. Cancer Res. 1999;59(7):1428-32.

31. Thomsen C, Grundevik P, Elias P, Stahlberg A, Aman P. A conserved N-terminal motif is required for complex formation between FUS, EWSR1, TAF15 and their oncogenic fusion proteins. FASEB J. 2013;27(12):4965-74.

32. Kovar H, Aryee D, Zoubek A. The Ewing family of tumors and the search for the Achilles' heel. Curr Opin Oncol. 1999;11(4):275-84.

33. May WA, Gishizky ML, Lessnick SL, Lunsford LB, Lewis BC, Delattre O, et al. Ewing sarcoma 11;22 translocation produces a chimeric transcription factor that requires the DNA-binding domain encoded by FLI1 for transformation. Proc Natl Acad Sci U S A. 1993;90(12):5752-6.

34. Castillero-Trejo Y, Eliazer S, Xiang L, Richardson JA, Ilaria RL, Jr. Expression of the EWS/FLI-1 oncogene in murine primary bone-derived cells Results in EWS/FLI-1-dependent, ewing sarcoma-like tumors. Cancer Res. 2005;65(19):8698-705.

35. Sohn EJ, Li H, Reidy K, Beers LF, Christensen BL, Lee SB. EWS/FLI1 oncogene activates caspase 3 transcription and triggers apoptosis in vivo. Cancer Res. 2010;70(3):1154-63.

36. Lessnick SL, Braun BS, Denny CT, May WA. Multiple domains mediate transformation by the Ewing's sarcoma EWS/FLI-1 fusion gene. Oncogene. 1995;10(3):423-31.

37. May WA, Lessnick SL, Braun BS, Klemsz M, Lewis BC, Lunsford LB, et al. The Ewing's sarcoma EWS/FLI-1 fusion gene encodes a more potent transcriptional activator and is a more powerful transforming gene than FLI-1. Mol Cell Biol. 1993;13(12):7393-8.

38. Riggi N, Cironi L, Provero P, Suva ML, Kaloulis K, Garcia-Echeverria C, et al. Development of Ewing's sarcoma from primary bone marrow-derived mesenchymal progenitor cells. Cancer Res. 2005;65(24):11459-68.

39. Riggi N, Suva ML, Suva D, Cironi L, Provero P, Tercier S, et al. EWS-FLI-1 expression triggers a Ewing's sarcoma initiation program in primary human mesenchymal stem cells. Cancer Res. 2008;68(7):2176-85.

40. Torchia EC, Boyd K, Rehg JE, Qu C, Baker SJ. EWS/FLI-1 induces rapid onset of myeloid/erythroid leukemia in mice. Mol Cell Biol. 2007;27(22):7918-34.

41. Leacock SW, Basse AN, Chandler GL, Kirk AM, Rakheja D, Amatruda JF. A zebrafish transgenic model of Ewing's sarcoma reveals conserved mediators of EWS-FLI1 tumorigenesis. Dis Model Mech. 2012;5(1):95-106.

42. Bailly RA, Bosselut R, Zucman J, Cormier F, Delattre O, Roussel M, et al. DNA-binding and transcriptional activation properties of the EWS-FLI-1 fusion protein resulting from the t(11;22) translocation in Ewing sarcoma. Mol Cell Biol. 1994;14(5):3230-41.

43. Braun BS, Frieden R, Lessnick SL, May WA, Denny CT. Identification of target genes for the Ewing's sarcoma EWS/FLI fusion protein by representational difference analysis. Mol Cell Biol. 1995;15(8):4623-30.

44. Hahm KB, Cho K, Lee C, Im YH, Chang J, Choi SG, et al. Repression of the gene encoding the TGF-beta type II receptor is a major target of the EWS-FLI1 oncoprotein. Nat Genet. 1999;23(2):222-7.

45. Gangwal K, Sankar S, Hollenhorst PC, Kinsey M, Haroldsen SC, Shah AA, et al. Microsatellites as EWS/FLI response elements in Ewing's sarcoma. Proc Natl Acad Sci U S A. 2008;105(29):10149-54.

46. Riggi N, Knoechel B, Gillespie SM, Rheinbay E, Boulay G, Suva ML, et al. EWS-FLI1 utilizes divergent chromatin remodeling mechanisms to directly activate or repress enhancer elements in Ewing sarcoma. Cancer Cell. 2014;26(5):668-81.

47. Guillon N, Tirode F, Boeva V, Zynovyev A, Barillot E, Delattre O. The oncogenic EWS-FLI1 protein binds in vivo GGAA microsatellite sequences with potential transcriptional activation function. PLoS One. 2009;4(3):e4932.

48. Gangwal K, Close D, Enriquez CA, Hill CP, Lessnick SL. Emergent Properties of EWS/FLI Regulation via GGAA Microsatellites in Ewing's Sarcoma. Genes Cancer. 2010;1(2):177-87.

49. Li KK, Lee KA. Transcriptional activation by the Ewing's sarcoma (EWS) oncogene can be cis-repressed by the EWS RNA-binding domain. J Biol Chem. 2000;275(30):23053-8.

50. Alex D, Lee KA. RGG-boxes of the EWS oncoprotein repress a range of transcriptional activation domains. Nucleic Acids Res. 2005;33(4):1323-31.

51. Kauer M, Ban J, Kofler R, Walker B, Davis S, Meltzer P, et al. A molecular function map of Ewing's sarcoma. PLoS One. 2009;4(4):e5415.

52. Prieur A, Tirode F, Cohen P, Delattre O. EWS/FLI-1 silencing and gene profiling of Ewing cells reveal downstream oncogenic pathways and a crucial role for repression of insulin-like growth factor binding protein 3. Mol Cell Biol. 2004;24(16):7275-83.

53. Nakatani F, Tanaka K, Sakimura R, Matsumoto Y, Matsunobu T, Li X, et al. Identification of p21WAF1/CIP1 as a direct target of EWS-Fli1 oncogenic fusion protein. J Biol Chem. 2003;278(17):15105-15.

54. Agra N, Cidre F, Garcia-Garcia L, de la Parra J, Alonso J. Lysyl oxidase is downregulated by the EWS/FLI1 oncoprotein and its propeptide domain displays tumor supressor activities in Ewing sarcoma cells. PLoS One. 2013;8(6):e66281.

55. Cironi L, Riggi N, Provero P, Wolf N, Suva ML, Suva D, et al. IGF1 is a common target gene of Ewing's sarcoma fusion proteins in mesenchymal progenitor cells. PLoS One. 2008;3(7):e2634.

56. Kennedy AL, Vallurupalli M, Chen L, Crompton B, Cowley G, Vazquez F, et al. Functional, chemical genomic, and super-enhancer screening identify sensitivity to cyclin D1/CDK4 pathway inhibition in Ewing sarcoma. Oncotarget. 2015;6(30):30178-93.

57. Richter GH, Plehm S, Fasan A, Rossler S, Unland R, Bennani-Baiti IM, et al. EZH2 is a mediator of EWS/FLI1 driven tumor growth and metastasis blocking endothelial and neuro-ectodermal differentiation. Proc Natl Acad Sci U S A. 2009;106(13):5324-9.

58. Ren C, Ren T, Yang K, Wang S, Bao X, Zhang F, et al. Inhibition of SOX2 induces cell apoptosis and G1/S arrest in Ewing's sarcoma through the PI3K/Akt pathway. J Exp Clin Cancer Res. 2016;35:44.

59. Hu-Lieskovan S, Heidel JD, Bartlett DW, Davis ME, Triche TJ. Sequence-specific knockdown of EWS-FLI1 by targeted, nonviral delivery of small interfering RNA inhibits

tumor growth in a murine model of metastatic Ewing's sarcoma. Cancer Res. 2005;65(19):8984-92.

60. Chansky HA, Barahmand-Pour F, Mei Q, Kahn-Farooqi W, Zielinska-Kwiatkowska A, Blackburn M, et al. Targeting of EWS/FLI-1 by RNA interference attenuates the tumor phenotype of Ewing's sarcoma cells in vitro. J Orthop Res. 2004;22(4):910-7.

61. Torchia EC, Jaishankar S, Baker SJ. Ewing tumor fusion proteins block the differentiation of pluripotent marrow stromal cells. Cancer Res. 2003;63(13):3464-8.

62. Sizemore GM, Pitarresi JR, Balakrishnan S, Ostrowski MC. The ETS family of oncogenic transcription factors in solid tumours. Nat Rev Cancer. 2017;17(6):337-51.

63. Todorova R. Disordered binding regions of Ewing's sarcoma fusion proteins. Bioorg Khim. 2014;40(1):20-30.

64. Todorova R. Structure-function based molecular relationships in Ewing's sarcoma. Biomed Res Int. 2015;2015:798426.

65. Erkizan HV, Kong Y, Merchant M, Schlottmann S, Barber-Rotenberg JS, Yuan L, et al. A small molecule blocking oncogenic protein EWS-FLI1 interaction with RNA helicase A inhibits growth of Ewing's sarcoma. Nat Med. 2009;15(7):750-6.

66. Li YJ, Zhao X, Vecchiarelli-Federico LM, Li Y, Datti A, Cheng Y, et al. Drug-mediated inhibition of Fli-1 for the treatment of leukemia. Blood Cancer J. 2012;2(1):e54.

67. Turner DP, Watson DK. ETS transcription factors: oncogenes and tumor suppressor genes as therapeutic targets for prostate cancer. Expert Rev Anticancer Ther. 2008;8(1):33-42.

68. Takigami I, Ohno T, Kitade Y, Hara A, Nagano A, Kawai G, et al. Synthetic siRNA targeting the breakpoint of EWS/Fli-1 inhibits growth of Ewing sarcoma xenografts in a mouse model. Int J Cancer. 2011;128(1):216-26.

69. Hensel T, Giorgi C, Schmidt O, Calzada-Wack J, Neff F, Buch T, et al. Targeting the EWS-ETS transcriptional program by BET bromodomain inhibition in Ewing sarcoma. Oncotarget. 2016;7(2):1451-63.

70. Jacques C, Lamoureux F, Baud'huin M, Rodriguez Calleja L, Quillard T, Amiaud J, et al. Targeting the epigenetic readers in Ewing sarcoma inhibits the oncogenic transcription factor EWS/Fli1. Oncotarget. 2016;7(17):24125-40.

71. Stegmaier K, Wong JS, Ross KN, Chow KT, Peck D, Wright RD, et al. Signature-based small molecule screening identifies cytosine arabinoside as an EWS/FLI modulator in Ewing sarcoma. PLoS Med. 2007;4(4):e122.

72. Andre N, Verschuur A, Rome A, Coze C, Gentet JC, Padovani L. Low dose cytarabine in patients with relapsed or refractory Ewing sarcoma. Pediatr Blood Cancer. 2009;53(2):238.

73. Lessnick SL, Ladanyi M. Molecular pathogenesis of Ewing sarcoma: new therapeutic and transcriptional targets. Annu Rev Pathol. 2012;7:145-59.

74. Lee SB, Frattini V, Bansal M, Castano AM, Sherman D, Hutchinson K, et al. An ID2-dependent mechanism for VHL inactivation in cancer. Nature. 2016;529(7585):172-7.

75. Lee SH, Chen T, Zhou J, Hofmann J, Bepler G. Protein kinase C-beta gene variants, pathway activation, and enzastaurin activity in lung cancer. Clin Lung Cancer. 2010;11(3):169-75.

76. Huang X, Du X, Li Y. The role of BCL11B in hematological malignancy. Exp Hematol Oncol. 2012;1(1):22.

77. Amaral AT, Garofalo C, Frapolli R, Manara MC, Mancarella C, Uboldi S, et al. Trabectedin efficacy in Ewing sarcoma is greatly increased by combination with anti-IGF signaling agents. Clin Cancer Res. 2015;21(6):1373-82.

78. Selvanathan SP, Graham GT, Erkizan HV, Dirksen U, Natarajan TG, Dakic A, et al. Oncogenic fusion protein EWS-FLI1 is a network hub that regulates alternative splicing. Proc Natl Acad Sci U S A. 2015;112(11):E1307-16.

79. Brenner JC, Feng FY, Han S, Patel S, Goyal SV, Bou-Maroun LM, et al. PARP-1 inhibition as a targeted strategy to treat Ewing's sarcoma. Cancer Res. 2012;72(7):1608-13.

80. Petermann R, Mossier BM, Aryee DN, Khazak V, Golemis EA, Kovar H. Oncogenic EWS-Fli1 interacts with hsRPB7, a subunit of human RNA polymerase II. Oncogene. 1998;17(5):603-10.

81. Choy E, Butrynski JE, Harmon DC, Morgan JA, George S, Wagner AJ, et al. Phase II study of olaparib in patients with refractory Ewing sarcoma following failure of standard chemotherapy. BMC Cancer. 2014;14:813.

82. Hong SH, Youbi SE, Hong SP, Kallakury B, Monroe P, Erkizan HV, et al. Pharmacokinetic modeling optimizes inhibition of the 'undruggable' EWS-FLI1 transcription factor in Ewing Sarcoma. Oncotarget. 2014;5(2):338-50.

83. Lazo JS, Sharlow ER. Drugging Undruggable Molecular Cancer Targets. Annu Rev Pharmacol Toxicol. 2016;56:23-40.

84. Grohar PJ, Griffin LB, Yeung C, Chen QR, Pommier Y, Khanna C, et al. Ecteinascidin 743 interferes with the activity of EWS-FLI1 in Ewing sarcoma cells. Neoplasia. 2011;13(2):145-53.

85. Grohar PJ, Woldemichael GM, Griffin LB, Mendoza A, Chen QR, Yeung C, et al. Identification of an inhibitor of the EWS-FLI1 oncogenic transcription factor by high-throughput screening. J Natl Cancer Inst. 2011;103(12):962-78.

86. Osgood CL, Maloney N, Kidd CG, Kitchen-Goosen S, Segars L, Gebregiorgis M, et al. Identification of Mithramycin Analogues with Improved Targeting of the EWS-FLI1 Transcription Factor. Clin Cancer Res. 2016;22(16):4105-18.

87. Youngken HW, Society MT. Food-drugs from the Sea: Proceedings, 1969: Marine Technology Society; 1970.

88. Wright AE FD, Gunawardana PG, Gunasekara SP, Koehn FE, McConnell OJ. Antitumor tetrahydroisoquinoline alkaloids from the colonial ascidian Ecteinascidia turbinata. Journal of Organic Chemistry. 1990;55:4508-12.

89. Corey EJ GD, Kania RS. Enantioselective Total Synthesis of Ecteinascidin 743. Journal of the American Chemical Society. 1996;118(September 25, 1996):9202-3.

90. Li L, Deng W, Song J, Ding W, Zhao QF, Peng C, et al. Characterization of the saframycin A gene cluster from Streptomyces lavendulae NRRL 11002 revealing a nonribosomal peptide synthetase system for assembling the unusual tetrapeptidyl skeleton in an iterative manner. J Bacteriol. 2008;190(1):251-63.

91. Soares DG, Escargueil AE, Poindessous V, Sarasin A, de Gramont A, Bonatto D, et al. Replication and homologous recombination repair regulate DNA double-strand break formation by the antitumor alkylator ecteinascidin 743. Proc Natl Acad Sci U S A. 2007;104(32):13062-7.

92. Pommier Y, Kohlhagen G, Bailly C, Waring M, Mazumder A, Kohn KW. DNA sequence- and structure-selective alkylation of guanine N2 in the DNA minor groove by ecteinascidin 743, a potent antitumor compound from the Caribbean tunicate Ecteinascidia turbinata. Biochemistry. 1996;35(41):13303-9.

93. Hurley LH, Zewail-Foote M. The antitumor agent ecteinascidin 743: characterization of its covalent DNA adducts and chemical stability. Adv Exp Med Biol. 2001;500:289-99.

94. David-Cordonnier MH, Gajate C, Olmea O, Laine W, de la Iglesia-Vicente J, Perez C, et al. DNA and non-DNA targets in the mechanism of action of the antitumor drug trabectedin. Chem Biol. 2005;12(11):1201-10.

95. Cuevas C, Francesch A. Development of Yondelis (trabectedin, ET-743). A semisynthetic process solves the supply problem. Nat Prod Rep. 2009;26(3):322-37.

96. Erba E, Cavallaro E, Damia G, Mantovani R, Di Silvio A, Di Francesco AM, et al. The unique biological features of the marine product Yondelis (ET-743, trabectedin) are shared by its analog ET-637, which lacks the C ring. Oncol Res. 2004;14(11-12):579-87.

97. Takebayashi Y, Pourquier P, Zimonjic DB, Nakayama K, Emmert S, Ueda T, et al. Antiproliferative activity of ecteinascidin 743 is dependent upon transcription-coupled nucleotide-excision repair. Nat Med. 2001;7(8):961-6.

98. Stevens EV, Nishizuka S, Antony S, Reimers M, Varma S, Young L, et al. Predicting cisplatin and trabectedin drug sensitivity in ovarian and colon cancers. Mol Cancer Ther. 2008;7(1):10-8.

99. Uboldi S, Bernasconi S, Romano M, Marchini S, Fuso Nerini I, Damia G, et al. Characterization of a new trabectedin-resistant myxoid liposarcoma cell line that shows collateral sensitivity to methylating agents. Int J Cancer. 2012;131(1):59-69.

100. Colmegna B, Uboldi S, Frapolli R, Licandro SA, Panini N, Galmarini CM, et al. Increased sensitivity to platinum drugs of cancer cells with acquired resistance to trabectedin. Br J Cancer. 2015;113(12):1687-93.

101. Marteijn JA, Lans H, Vermeulen W, Hoeijmakers JH. Understanding nucleotide excision repair and its roles in cancer and ageing. Nat Rev Mol Cell Biol. 2014;15(7):465-81.

102. Scharer OD. XPG: its products and biological roles. Adv Exp Med Biol. 2008;637:83-92.

103. Herrero AB, Martin-Castellanos C, Marco E, Gago F, Moreno S. Cross-talk between nucleotide excision and homologous recombination DNA repair pathways in the mechanism of action of antitumor trabectedin. Cancer Res. 2006;66(16):8155-62.

104. Tavecchio M, Simone M, Erba E, Chiolo I, Liberi G, Foiani M, et al. Role of homologous recombination in trabectedin-induced DNA damage. Eur J Cancer. 2008;44(4):609-18.

105. Bonfanti M, La Valle E, Fernandez Sousa Faro JM, Faircloth G, Caretti G, Mantovani R, et al. Effect of ecteinascidin-743 on the interaction between DNA binding proteins and DNA. Anticancer Drug Des. 1999;14(3):179-86.

106. Grosso F, Jones RL, Demetri GD, Judson IR, Blay JY, Le Cesne A, et al. Efficacy of trabectedin (ecteinascidin-743) in advanced pretreated myxoid liposarcomas: a retrospective study. Lancet Oncol. 2007;8(7):595-602.

107. Schoffski P, Dumez H, Wolter P, Stefan C, Wozniak A, Jimeno J, et al. Clinical impact of trabectedin (ecteinascidin-743) in advanced/metastatic soft tissue sarcoma. Expert Opin Pharmacother. 2008;9(9):1609-18.

108. Grosso F, Sanfilippo R, Virdis E, Piovesan C, Collini P, Dileo P, et al. Trabectedin in myxoid liposarcomas (MLS): a long-term analysis of a single-institution series. Ann Oncol. 2009;20(8):1439-44.

109. Le Cesne A, Cresta S, Maki RG, Blay JY, Verweij J, Poveda A, et al. A retrospective analysis of antitumour activity with trabectedin in translocation-related sarcomas. Eur J Cancer. 2012;48(16):3036-44.

110. Forni C, Minuzzo M, Virdis E, Tamborini E, Simone M, Tavecchio M, et al. Trabectedin (ET-743) promotes differentiation in myxoid liposarcoma tumors. Mol Cancer Ther. 2009;8(2):449-57.

111. Demetri GD, von Mehren M, Jones RL, Hensley ML, Schuetze SM, Staddon A, et al. Efficacy and Safety of Trabectedin or Dacarbazine for Metastatic Liposarcoma or Leiomyosarcoma After Failure of Conventional Chemotherapy: Results of a Phase III Randomized Multicenter Clinical Trial. J Clin Oncol. 2016;34(8):786-93.

112. Lau L, Supko JG, Blaney S, Hershon L, Seibel N, Krailo M, et al. A phase I and pharmacokinetic study of ecteinascidin-743 (Yondelis) in children with refractory solid tumors. A Children's Oncology Group study. Clin Cancer Res. 2005;11(2 Pt 1):672-7.

113. Baruchel S, Pappo A, Krailo M, Baker KS, Wu B, Villaluna D, et al. A phase 2 trial of trabectedin in children with recurrent rhabdomyosarcoma, Ewing sarcoma and non-rhabdomyosarcoma soft tissue sarcomas: a report from the Children's Oncology Group. Eur J Cancer. 2012;48(4):579-85.

114. Grohar PJ, Segars LE, Yeung C, Pommier Y, D'Incalci M, Mendoza A, et al. Dual targeting of EWS-FLI1 activity and the associated DNA damage response with trabectedin and SN38 synergistically inhibits Ewing sarcoma cell growth. Clin Cancer Res. 2014;20(5):1190-203.

115. Scott JD, Williams RM. Chemistry and biology of the tetrahydroisoquinoline antitumor antibiotics. Chem Rev. 2002;102(5):1669-730.

116. Rinehart KL HT, Fregeau NL, Stroh JG, Keifer PA, Furong S, Li HL, Martin DG. Ecteinascidins 729, 743, 745, 759A, 759B, and 770: potent antitumor agents from the Caribbean tunicate Ecteinascidia turbinata. Journal of Organic Chemistry. 1990;55:4512-15.

117. Arai T, Takahashi K, Kubo A. New antibiotics saframycins A, B, C, D and E. J Antibiot (Tokyo). 1977;30(11):1015-8.

118. Lown JW, Joshua AV, Lee JS. Molecular mechanisms of binding and single-strand scission of deoxyribonucleic acid by the antitumor antibiotics saframycins A and C. Biochemistry. 1982;21(3):419-28.

119. Zewail-Foote M, Hurley LH. Ecteinascidin 743: a minor groove alkylator that bends DNA toward the major groove. J Med Chem. 1999;42(14):2493-7.

120. Takebayashi Y, Pourquier P, Yoshida A, Kohlhagen G, Pommier Y. Poisoning of human DNA topoisomerase I by ecteinascidin 743, an anticancer drug that selectively alkylates DNA in the minor groove. Proc Natl Acad Sci U S A. 1999;96(13):7196-201.

121. Takebayashi Y, Goldwasser F, Urasaki Y, Kohlhagen G, Pommier Y. Ecteinascidin 743 induces protein-linked DNA breaks in human colon carcinoma HCT116 cells and is cytotoxic independently of topoisomerase I expression. Clin Cancer Res. 2001;7(1):185-91.

122. Aune GJ, Takagi K, Sordet O, Guirouilh-Barbat J, Antony S, Bohr VA, et al. Von Hippel-Lindau-coupled and transcription-coupled nucleotide excision repair-dependent degradation of RNA polymerase II in response to trabectedin. Clin Cancer Res. 2008;14(20):6449-55.

123. Garcia-Rocha M, Garcia-Gravalos MD, Avila J. Characterisation of antimitotic products from marine organisms that disorganise the microtubule network: ecteinascidin 743, isohomohalichondrin-B and LL-15. Br J Cancer. 1996;73(8):875-83.

124. D'Incalci M, Badri N, Galmarini CM, Allavena P. Trabectedin, a drug acting on both cancer cells and the tumour microenvironment. Br J Cancer. 2014;111(4):646-50.

125. Perez-Losada J, Pintado B, Gutierrez-Adan A, Flores T, Banares-Gonzalez B, del Campo JC, et al. The chimeric FUS/TLS-CHOP fusion protein specifically induces liposarcomas in transgenic mice. Oncogene. 2000;19(20):2413-22.

126. Di Giandomenico S, Frapolli R, Bello E, Uboldi S, Licandro SA, Marchini S, et al. Mode of action of trabectedin in myxoid liposarcomas. Oncogene. 2014;33(44):5201-10.

127. Lo-Coco F, Di Donato L, Gimema, Schlenk RF, German-Austrian Acute Myeloid Leukemia Study G, Study Alliance L. Targeted Therapy Alone for Acute Promyelocytic Leukemia. N Engl J Med. 2016;374(12):1197-8.

128. Kovar H. Dr. Jekyll and Mr. Hyde: The Two Faces of the FUS/EWS/TAF15 Protein Family. Sarcoma. 2011;2011:837474.

129. Bachmaier R, Aryee DN, Jug G, Kauer M, Kreppel M, Lee KA, et al. O-GlcNAcylation is involved in the transcriptional activity of EWS-FLI1 in Ewing's sarcoma. Oncogene. 2009;28(9):1280-4.

130. Klevernic IV, Morton S, Davis RJ, Cohen P. Phosphorylation of Ewing's sarcoma protein (EWS) and EWS-Fli1 in response to DNA damage. Biochem J. 2009;418(3):625-34.

131. Sankar S, Lessnick SL. Promiscuous partnerships in Ewing's sarcoma. Cancer Genet. 2011;204(7):351-65.

132. Schlottmann S, Erkizan HV, Barber-Rotenberg JS, Knights C, Cheema A, Uren A, et al. Acetylation Increases EWS-FLI1 DNA Binding and Transcriptional Activity. Front Oncol. 2012;2:107.

133. Olsen JV, Ong SE, Mann M. Trypsin cleaves exclusively C-terminal to arginine and lysine residues. Mol Cell Proteomics. 2004;3(6):608-14.

134. Gutfreund H, Sturtevant JM. The Mechanism of Chymotrypsin-Catalyzed Reactions. Proc Natl Acad Sci U S A. 1956;42(10):719-28.

135. Huang H, Yu M, Akie TE, Moran TB, Woo AJ, Tu N, et al. Differentiation-dependent interactions between RUNX-1 and FLI-1 during megakaryocyte development. Mol Cell Biol. 2009;29(15):4103-15.

136. Schwartz JC, Cech TR, Parker RR. Biochemical Properties and Biological Functions of FET Proteins. Annu Rev Biochem. 2015;84:355-79.

137. Belyanskaya LL, Delattre O, Gehring H. Expression and subcellular localization of Ewing sarcoma (EWS) protein is affected by the methylation process. Exp Cell Res. 2003;288(2):374-81.

138. Araya N, Hiraga H, Kako K, Arao Y, Kato S, Fukamizu A. Transcriptional down-regulation through nuclear exclusion of EWS methylated by PRMT1. Biochem Biophys Res Commun. 2005;329(2):653-60.

139. Paronetto MP, Minana B, Valcarcel J. The Ewing sarcoma protein regulates DNA damage-induced alternative splicing. Mol Cell. 2011;43(3):353-68.

140. Guirouilh-Barbat J, Antony S, Pommier Y. Zalypsis (PM00104) is a potent inducer of gamma-H2AX foci and reveals the importance of the C ring of trabectedin for transcription-coupled repair inhibition. Mol Cancer Ther. 2009;8(7):2007-14.

141. Celeste A, Fernandez-Capetillo O, Kruhlak MJ, Pilch DR, Staudt DW, Lee A, et al. Histone H2AX phosphorylation is dispensable for the initial recognition of DNA breaks. Nat Cell Biol. 2003;5(7):675-9.

142. O'Leary J, Muggia FM. Camptothecins: a review of their development and schedules of administration. Eur J Cancer. 1998;34(10):1500-8.

143. Hande KR. The importance of drug scheduling in cancer chemotherapy: etoposide as an example. Stem Cells. 1996;14(1):18-24.

144. Slevin ML, Clark PI, Joel SP, Malik S, Osborne RJ, Gregory WM, et al. A randomized trial to evaluate the effect of schedule on the activity of etoposide in small-cell lung cancer. J Clin Oncol. 1989;7(9):1333-40.

145. Clark PI, Slevin ML, Joel SP, Osborne RJ, Talbot DI, Johnson PW, et al. A randomized trial of two etoposide schedules in small-cell lung cancer: the influence of pharmacokinetics on efficacy and toxicity. J Clin Oncol. 1994;12(7):1427-35.

146. Rodman JH, Abromowitch M, Sinkule JA, Hayes FA, Rivera GK, Evans WE. Clinical pharmacodynamics of continuous infusion teniposide: systemic exposure as a determinant of response in a phase I trial. J Clin Oncol. 1987;5(7):1007-14.

147. Forouzesh B, Hidalgo M, Chu Q, Mita A, Mita M, Schwartz G, et al. Phase I and pharmacokinetic study of trabectedin as a 1- or 3-hour infusion weekly in patients with advanced solid malignancies. Clin Cancer Res. 2009;15(10):3591-9.

148. Beumer JH, Rademaker-Lakhai JM, Rosing H, Lopez-Lazaro L, Beijnen JH, Schellens JH. Trabectedin (Yondelis, formerly ET-743), a mass balance study in patients with advanced cancer. Invest New Drugs. 2005;23(5):429-36.

149. Lowis SP, Newell DR, Pearson AD. Exposure and schedule dependency of etoposide in neuroblastoma and leukaemia cells in vitro. Eur J Cancer. 1995;31A(4):622-6.

150. Maison C, Almouzni G. HP1 and the dynamics of heterochromatin maintenance. Nat Rev Mol Cell Biol. 2004;5(4):296-304.

151. Noh KM, Maze I, Zhao D, Xiang B, Wenderski W, Lewis PW, et al. ATRX tolerates activity-dependent histone H3 methyl/phos switching to maintain repetitive element silencing in neurons. Proc Natl Acad Sci U S A. 2015;112(22):6820-7.

152. Muller-Ott K, Erdel F, Matveeva A, Mallm JP, Rademacher A, Hahn M, et al. Specificity, propagation, and memory of pericentric heterochromatin. Mol Syst Biol. 2014;10:746.

153. Bulut-Karslioglu A, De La Rosa-Velazquez IA, Ramirez F, Barenboim M, Onishi-Seebacher M, Arand J, et al. Suv39h-dependent H3K9me3 marks intact retrotransposons and silences LINE elements in mouse embryonic stem cells. Mol Cell. 2014;55(2):277-90.

154. Herzog J, von Klot-Heydenfeldt F, Jabar S, Ranft A, Rossig C, Dirksen U, et al. Trabectedin Followed by Irinotecan Can Stabilize Disease in Advanced Translocation-Positive Sarcomas with Acceptable Toxicity. Sarcoma. 2016;2016:7461783.

155. Demetri GD, Chawla SP, von Mehren M, Ritch P, Baker LH, Blay JY, et al. Efficacy and safety of trabectedin in patients with advanced or metastatic liposarcoma or leiomyosarcoma after failure of prior anthracyclines and ifosfamide: results of a randomized phase II study of two different schedules. J Clin Oncol. 2009;27(25):4188-96.

156. Leal JF, Martinez-Diez M, Garcia-Hernandez V, Moneo V, Domingo A, Bueren-Calabuig JA, et al. PM01183, a new DNA minor groove covalent binder with potent in vitro and in vivo anti-tumour activity. Br J Pharmacol. 2010;161(5):1099-110.

157. Yap TA, Cortes-Funes H, Shaw H, Rodriguez R, Olmos D, Lal R, et al. First-in-man phase I trial of two schedules of the novel synthetic tetrahydroisoquinoline alkaloid PM00104 (Zalypsis) in patients with advanced solid tumours. Br J Cancer. 2012;106(8):1379-85.

158. Leal JF, Garcia-Hernandez V, Moneo V, Domingo A, Bueren-Calabuig JA, Negri A, et al. Molecular pharmacology and antitumor activity of Zalypsis in several human cancer cell lines. Biochem Pharmacol. 2009;78(2):162-70.

159. Ocio EM, Maiso P, Chen X, Garayoa M, Alvarez-Fernandez S, San-Segundo L, et al. Zalypsis: a novel marine-derived compound with potent antimyeloma activity that reveals high sensitivity of malignant plasma cells to DNA double-strand breaks. Blood. 2009;113(16):3781-91.

160. Petek BJ, Jones RL. PM00104 (Zalypsis(R)): a marine derived alkylating agent. Molecules. 2014;19(8):12328-35.

161. Jones RL, Ferrari S, Blay JY, Navid F, Lardelli P, Alfaro V, et al. A Phase II multicenter, open-label, clinical and pharmokinetic trial of PM00104 in patients with advanced Ewing Family of Tumors. Invest New Drugs. 2014;32(1):171-7.

162. Elez ME, Tabernero J, Geary D, Macarulla T, Kang SP, Kahatt C, et al. First-in-human phase I study of Lurbinectedin (PM01183) in patients with advanced solid tumors. Clin Cancer Res. 2014;20(8):2205-14.

163. Paz-Ares L, Forster M, Boni V, Szyldergemajn S, Corral J, Turnbull S, et al. Phase I clinical and pharmacokinetic study of PM01183 (a tetrahydroisoquinoline, Lurbinectedin) in combination with gemcitabine in patients with advanced solid tumors. Invest New Drugs. 2016.

164. Hancock JD, Lessnick SL. A transcriptional profiling meta-analysis reveals a core EWS-FLI gene expression signature. Cell Cycle. 2008;7(2):250-6.

165. Boro A, Pretre K, Rechfeld F, Thalhammer V, Oesch S, Wachtel M, et al. Small-molecule screen identifies modulators of EWS/FLI1 target gene expression and cell survival in Ewing's sarcoma. Int J Cancer. 2012;131(9):2153-64.

166. Proia DA, Kuperwasser C. Reconstruction of human mammary tissues in a mouse model. Nat Protoc. 2006;1(1):206-14.

167. Saint-Andre V, Federation AJ, Lin CY, Abraham BJ, Reddy J, Lee TI, et al. Models of human core transcriptional regulatory circuitries. Genome Res. 2016;26(3):385-96.

168. Teven CM, Liu X, Hu N, Tang N, Kim SH, Huang E, et al. Epigenetic regulation of mesenchymal stem cells: a focus on osteogenic and adipogenic differentiation. Stem Cells Int. 2011;2011:201371.

169. Suva ML, Riggi N, Bernstein BE. Epigenetic reprogramming in cancer. Science. 2013;339(6127):1567-70.

170. Perez-Campo FM, Riancho JA. Epigenetic Mechanisms Regulating Mesenchymal Stem Cell Differentiation. Curr Genomics. 2015;16(6):368-83.

171. Asp P, Blum R, Vethantham V, Parisi F, Micsinai M, Cheng J, et al. Genome-wide remodeling of the epigenetic landscape during myogenic differentiation. Proc Natl Acad Sci U S A. 2011;108(22):E149-58.

172. Herlofsen SR, Bryne JC, Hoiby T, Wang L, Issner R, Zhang X, et al. Genome-wide map of quantified epigenetic changes during in vitro chondrogenic differentiation of primary human mesenchymal stem cells. BMC Genomics. 2013;14:105.

173. Eisenhauer EA, Therasse P, Bogaerts J, Schwartz LH, Sargent D, Ford R, et al. New response evaluation criteria in solid tumours: revised RECIST guideline (version 1.1). Eur J Cancer. 2009;45(2):228-47.

174. Osgood CL, Tantawy MN, Maloney N, Madaj ZB, Peck A, Boguslawski E, et al. 18F-FLT Positron Emission Tomography (PET) is a Pharmacodynamic Marker for EWS-FLI1 Activity and Ewing Sarcoma. Sci Rep. 2016;6:33926.

175. Marinello J, Chillemi G, Bueno S, Manzo SG, Capranico G. Antisense transcripts enhanced by camptothecin at divergent CpG-island promoters associated with bursts of topoisomerase I-DNA cleavage complex and R-loop formation. Nucleic Acids Res. 2013;41(22):10110-23.

176. Liao Y, Smyth GK, Shi W. The Subread aligner: fast, accurate and scalable read mapping by seed-and-vote. Nucleic Acids Res. 2013;41(10):e108.

177. Law CW, Chen Y, Shi W, Smyth GK. voom: Precision weights unlock linear model analysis tools for RNA-seq read counts. Genome Biol. 2014;15(2):R29.

178. Ritchie ME, Phipson B, Wu D, Hu Y, Law CW, Shi W, et al. limma powers differential expression analyses for RNA-sequencing and microarray studies. Nucleic Acids Res. 2015;43(7):e47.